Hydrogen Atom Adducts to Nitrobenzene: Formation of the Phenylnitronic Radical in the Gas Phase and Energetics of Wheland Intermediates

Miroslav Polášek and František Tureček*

Contribution from the Department of Chemistry, Bagley Hall, Box 351700, University of Washington, Seattle, Washington 98195-1700

Received April 7, 2000

Abstract: The phenylnitronic radical (**1**) was prepared in the gas phase by collisional electron transfer to stable $C_6H_5NO_2H^+$ cation ($\mathbf{1}^+$) and found to be stable on the microsecond time scale. The major unimolecular dissociation of **1** was loss of OH radical to form nitrosobenzene as determined by variable-time neutralization−reionization mass spectrometry. Ab initio calculations at the effective QCISD(T)/6-311+G(3df,2p) level and combined Møller−Plesset and density functional theory calculations identified loss of OH as the lowest-energy dissociation of **1** that proceeded at the thermochemical threshold with no reverse activation barrier. Dissociations of **1** by loss of *syn*- and *anti*-HONO and a hydrogen atom were more endothermic than loss of OH and had activation barriers above the thermochemical thresholds. The internal energy of **1** formed by electron transfer in the ground electronic state (*X*) was insufficient to cause the observed dissociations. The dissociations are postulated to take place from the metastable excited electronic *B* state formed by vertical electron transfer. Wheland intermediates for hydrogen atom additions to the *ortho* (**2**), *meta* (**3**), *para* (**4**), and *ipso* (**5**) positions in nitrobenzene were calculated to be 75, 98, 78, and 101 kJ mol^{-1} less stable than **1**. Radicals **2**−**4** existed in substantially deep potential energy wells to allow their generation as transient intermediates. Radical **5** resided in a shallow potential energy minimum and was predicted to dissociate exothermically to benzene and NO_2. Relative thermal rate constants for hydrogen atom additions to nitrobenzene were calculated and found to correlate with the regioselectivities for additions of other radicals.

Introduction

Additions of small radicals to aromatic compounds have been of much interest because of their role in processes as diverse as tropospheric oxidations,[1] oxidative damage at tyrosine and tryptophan residues in proteins,[2] and decomposition of energetic materials.[3] In contrast, less is known about radical adducts to aromatic compounds carrying electronegative substitutents, such as the cyano and nitro groups.[4] This is despite the fact that nitroaromatic compounds are important biologically active pollutants and their metabolic reduction[5] and tropospheric degradation have been of interest.[6] A kinetic study of the nitrobenzene-hydroxyl radical reaction showed that nitrobenzene was less reactive than benzene by a factor of 2.[7]

Following Wheland's prediction[8] that the *para* and *ortho* positions should be more reactive than the *meta* position, the reactivity of nitrobenzene toward radical additions and the properties of radical intermediates have been studied at various levels of theory.[9] Wheland[8] and later Weiss and co-workers[10] postulated the existence of transient intermediates (Wheland intermediates[11]) formed by radical addition to the benzene ring, as illustrated for hydrogen atom adducts **1**−**5** in Scheme 1.

Scheme 1

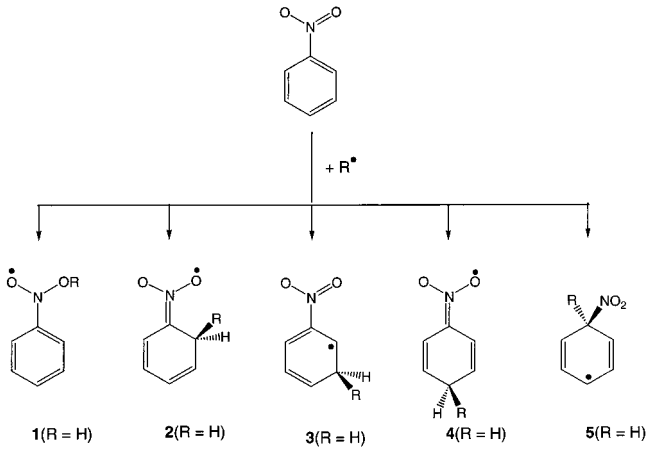

* Author for correspondence. Telephone: (206) 685-2041. Fax: (206) 685−3478. E-mail: turecek@chem.washington.edu.

(1) Atkinson, R. *Gas-Phase Tropospheric Chemistry*, *J. Phys. Chem. Ref. Data, Monograph No. 2*; American Chemical Society: Woodbury, NY, 1994.

(2) Richter, C. In *Free Radical Toxicology*; Wallace, K. B., Ed.; Taylor and Francis: Washington, DC, 1997.

(3) Brill, T. B.; James, K. J. *Chem. Rev.* **1993**, *93*, 2667.

(4) Urbanski, T. In *The Chemistry of the Nitro and Nitroso Groups*; Feuer, H., Ed.; Wiley-Interscience: New York, 1970; pp 64−73.

(5) (a) Kalhorn, T.; Becker, A. R.; Sternson, L. A. *Bioorg. Chem.* **1981**, *10*, 144. (b) Becker, A. R.; Sternoson, L. A. *Proc. Natl. Acad. Sci. U.S.A.* **1981**, *78*, 2003.

(6) Knispel, R.; Koch, R.; Siese, M.; Zetsch, C. *Ber. Bunsen-Ges. Phys. Chem.* **1990**, *94*, 1375.

(7) Arnts, R. R.; Seila, R. L.; Bufalini, J. J. *J. Air Pollut. Control Assoc.* **1989**, *39*, 453.

(8) Wheland, G. W. *J. Am. Chem. Soc.* **1942**, *64*, 900.

(9) (a) Shashin, S. S.; Rykova, E. A. *J. Mol. Struct. (THEOCHEM)* **1994**, *311*, 175. (b) Fabian, J.; Bleisch, S.; Domschke, G.; Mayer, R. *Z. Chem.* **1981**, 21, 265. (c) Ladik, J.; Biczo, G.; Kende, I.; Sumegi, L. *Acta Chim. Sci. Hung.* **1969**, *61*, 381.

(10) Loebl, H.; Stein, G.; Weiss, *J. Chem. Soc.* **1949**, 2074.

(11) March, J. *Advanced Organic Chemistry*, 3rd ed.; Wiley: New York, 1985; p 448.

10.1021/ja001229h CCC: $19.00
Published on Web 09/16/2000

Scheme 2

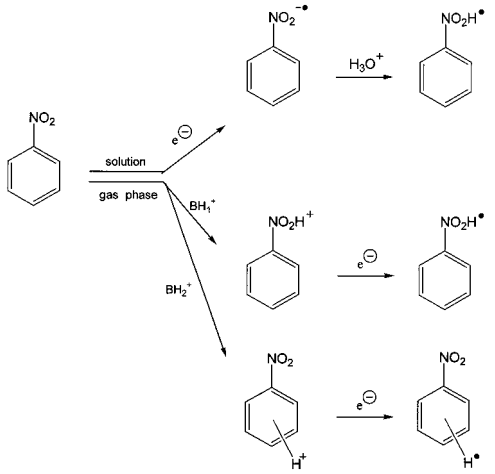

Hydroxyl radical addition to nitrobenzene was found to produce *o*-, *m*-, and *p*-nitrophenol, presumably via transient intermediates of the type shown in Scheme 1. Addition to nitrobenzene of methyl radicals produced by thermolysis of *tert*-butylperoxide formed mostly *o*- and *p*-nitrotoluene,[12] bearing out Wheland's predictions. The reactivity toward radical additions of the *ipso*-position and the nitro group has not been studied and their role in the radical chemistry of nitrobenzene is unclear. Recently, alkylation of *p*-dinitrobenzene with trialkylboranes has been interpreted as involving an alkyl radical addition step,[13] and nucleophilic substitutions in nitroaromates were considered to include radical intermediates.[14]

The phenylnitronic radical (**1**) corresponding to a hydrogen atom adduct to the nitro group in nitrobenzene has been postulated to arise by protonation of an anion-radical produced by electrochemical reduction[15a−f] or pulse radiolysis of nitrobenzene in protic solution[16a−c] (Scheme 2). The evidence for the transient formation of **1** was inferred from the changes in the absorption spectrum that showed two maxima at $\lambda = 418$ and 460 nm, which were blue-shifted by 10 nm from those of the nitrobenzene anion-radical.[16,17] In contrast, Cercek concluded from his pulse radiolysis kinetic measurements that hydrogen atom addition in nitrobenzene occurred in the ring to yield a nitrocyclohexadienyl radical.[18] Photolysis of nitrobenzene in tetrahydrofuran as a hydrogen atom donor resulted in the formation of transient radicals that were tentatively assigned structure **1** on the basis of electron paramagnetic resonance (EPR) spectra.[19] However, tetrahydrofuran adducts to nitrobenzene were also detected that complicated the interpretation of the EPR spectra.[19b]

Why does nitrobenzene exhibit different regioselectivities in radical and electrophilic additions? To answer this question we now study the energetics of nitrobenzene radicals and the activation energies of radical additions. Hydrogen atom additions represent the simplest models for radical additions to nitroaromates that can be tackled by experiment and theory. In this work we prepare radical **1** in the gas phase and study its unimolecular dissociations using the methods of neutralization−reionization mass spectrometry (NRMS),[20] including temporal resolution of radical reactions by variable-time NRMS.[21] Our approach starts with protonation of nitrobenzene in the gas-phase using an acid that targets selectively the nitro group to produce stable ions $\mathbf{1}^+$ (BH_1^+, Scheme 2) or using stronger acids that are capable of protonating the less basic ring positions (BH_2^+). Stable ions $\mathbf{1}^+$ are accelerated to a high velocity (113 750 m s^{-1}) and discharged by fast electron transfer ($<10^{-14}$ s) from dimethyl disulfide during a glancing collision. This approach is formally the reverse of the electrochemical reduction in which electron addition precedes protonation. To obtain a comprehensive view of hydrogen atom adducts to nitrobenzene, including relative isomer energies, dissociation energies and isomerization barriers, we carried out ab initio and density functional theory calculations at a high level of theory. The energy data are used to assess the kinetics of competitive unimolecular dissociations and the branching ratios in hydrogen atom additions to nitrobenzene. Dissociation mechanisms were studied using a series of deuterium-labeled radicals (**1a**−**1e**).

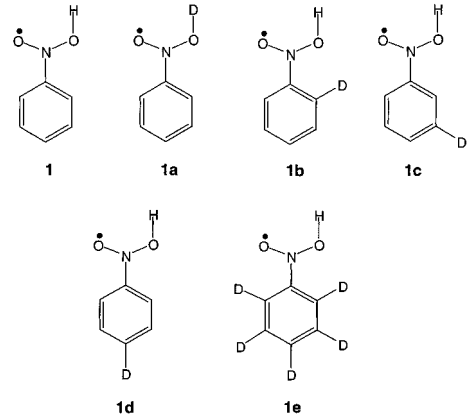

Experimental Section

Methods. Measurements were carried out on a tandem quadrupole acceleration−deceleration mass spectrometer described previously.[22] Precursor ions were generated in a tight chemical ionization (CI) source. Typical ionization conditions were as follows: electron energy 100 eV, emission current 1−2 mA, temperature 280−300 °C, ion source potential 80 V. CH_4, CD_4, CH_3OH, CD_3OD, CH_3CN, CD_3CN, and CH_3ONO_2 were used as reagent gases at pressures $1.0-1.5 \times 10^{-4}$ Torr as read on an ionization gauge located at the diffusion pump intake. CH_3O^- ions were generated by negative-ion chemical ionization (NCI) from a 90/10 mixture of CH_3OH and N_2O, H^- ions were prepared by dissociative electron capture in H_2. Typical NCI conditions were as follows: electron energy 200 eV, emission current 1 mA, temperature 280−300 °C, source potential −80 V. Electron ionization (EI) was used to generate cation-radicals $C_6H_5NO_2^{+\bullet}$, $C_6H_5NO^{+\bullet}$, and the phenyl

(12) Williams, G. H. In *Homolytic Aromatic Substitution*; Pergamon: Oxford, 1960; *loc. cit.* 90. See also ref 4.

(13) Shifman, A.; Palani, N.; Hoz, S. *Angew. Chem., Int. Ed.* **2000**, *39*, 944.

(14) Paradisi, C.; Scorrano, G. *Acc. Chem. Res.* **1999**, *32*, 958.

(15) (a) Karakus, C.; Zuman, P. *J. Electroanal. Chem.* **1995**, *396*, 499. (b) Zuman, P.; Fijalek, Z. *J. Org. Chem.* **1991**, *56*, 5486. (c) Rao, P. S.; Hayon, E. *Anal. Chem.* **1976**, *48*, 564. (d) Farnia, G.; Mengoli, G.; Vianello. E. *Sci. Chim.* **1967**, *37*, 668. (e) Geske, A. H.; Maki, D. H. *J. Am. Chem. Soc.* **1960**, *82*, 2671. (f) Geske, A. H.; Maki, D. H. *J. Chem. Phys.* **1960**, *33*, 825.

(16) (a) Asmus, K.-D.; Wigger, A.; Henglein, A. *Ber. Bunsen-Ges. Phys. Chem.* **1966**, *70*, 862. (b) Asmus, K.-D.; Cercek, B.; Ebert, M.; Henglein, A.; Wigger, A. *Trans. Faraday Soc.* **1967**, *63*, 2435. (c) Lilie, J.; Henglein, A. *Ber. Bunsen-Ges. Phys. Chem.* **1969**, *73*, 170.

(17) Iyer, S.; Capellos, C. In *Advances in Chemical Reaction Dynamics*; Rentzepis, P. M.; Capellos, C., Eds; Reidel: Amsterdam 1986; pp 405−414.

(18) Cercek, B. *Nature* **1971**, *234*, 159.

(19) (a) Ward, R. L. *J. Chem. Phys.* **1963**, *38*, 2588. (b) Chachaty, C.; Forchioni, A. *J. Chim. Phys., Phys. Chim. Biol.* **1968**, *65*, 1649.

(20) For most recent reviews see: (a) Zagorevskii, D.; Holmes, J. L. *Mass Spectrom. Rev.* **1999**, *18*, 87. (b) Schalley, C. A.; Hornung, G.; Schroder, D.; Schwarz, H. *Chem. Soc. Rev.* **1998**, *27*, 91. (c) Turecek, F. *J. Mass Spectrom.* **1998**, *33*, 779.

(21) (a) Kuhns, D. W.; Tran, T. B.; Shaffer, S. A.; Turecek, F. *J. Phys. Chem.* **1994**, *98*, 4845. (b) Kuhns D. W.; Turecek, F. *Org. Mass Spectrom.* **1994**, *29*, 463.

(22) Turecek, F.; Gu, M.; Shaffer, S. A. *J. Am. Soc. Mass Spectrom.* **1992**, *3*, 493.

cation $C_6H_5^+$ by dissociative ionization of nitrobenzene. Typical EI conditions were as follows: electron energy 70 eV, source temperature 280−300 °C, and sample pressure $5-8 \times 10^{-6}$ Torr. Stable precursor cations were passed through a quadrupole mass filter operated in the radio frequency-only mode, accelerated to the total kinetic energy of 8250 eV and neutralized in the collision cell floated at −8170 V. The precursor ion lifetimes were 30−40 μs. Dimethyl disulfide (DMDS) was admitted to the differentially pumped collision cell at a pressure such as to achieve 70% transmittance of the precursor ion beam. The ions and neutrals were allowed to drift to a four segment conduit,[23] where the ions were reflected by the first segment floated at +250 V. The neutral flight times in standard NRMS measurements were 5.3 μs. The fast neutral species were reionized in the second collision cell by collision with oxygen at a pressure adjusted such as to achieve 70% transmittance of the precursor ion beam. The ions formed in the second collision cell were decelerated, energy filtered, and analyzed by a quadrupole mass filter operated at unit mass resolution. The instrument was tuned daily to maximize the ion current of reionized $CS_2^{+\bullet}$. Typically, 40 repetitive scans were accumulated per spectrum, and each spectrum was reproduced at least three times over a period of several weeks. Variable-time measurements were carried out as described previously.[21] The neutral flight times that were used to evaluate the unimolecular dissociation kinetics were 0.51, 1.50, and 2.50 μs.

Collisionally activated dissociation (CAD) spectra were measured on a JEOL HX-110 double-focusing mass spectrometer of forward geometry (the electrostatic sector *E* precedes the magnet *B*). Collisions with air were monitored in the first field-free region at pressure to achieve 70% transmittance of the ion beam at 10 keV. The spectra were obtained by scanning *E* and *B* simultaneously while maintaining a constant *B*/*E* ratio (*B*/*E* linked scan).

Materials. Methane (Matheson, 99.97%), CD_4 (Cambridge Isotope Laboratories, 99% D), methanol (Aldrich), CD_3OD (Cambridge Isotope Laboratories, 99% D), CD_3CN (Cambridge Isotope Laboratories, 99% D), dimethyl disulfide (DMDS, Aldrich), nitrobenzene (Aldrich, 99%) and nitrobenzene-d_5 (Aldrich, 99% D), and nitrosobenzene (Aldrich) were used as received.

ortho-, *meta*-, and *para*-D-nitrobenzenes were synthesized from the corresponding nitroanilines (Aldrich) by diazotation with 1.5 equiv of $NaNO_2$ in D_2O/DCl at −5 °C followed by diazonium salt reduction with a 5-fold molar excess of D_3PO_2 (Aldrich, 99% D) at 0 °C overnight.[24] The products were extracted in ether, the solutions were decolorized with active charcoal, the solvent was distilled off, and the products were purified by vacuum distillation. The overall yields of distilled products were 50−70%. The product purity was verified by gas-chromatography mass spectrometry that showed 99% D_1 content in the labeled nitrobenzenes. Minor impurities were nitrosobenzene (<1%) and chloronitrobenzenes (<5%) that did not interfere in the mass spectrometric measurements. Methyl nitrate was prepared according to a literature procedure.[25]

Calculations. Standard ab initio and density functional theory calculations were performed using the Gaussian 98 suite of programs.[26] Geometries were optimized using Becke's hybrid functional (B3LYP)[27] and the 6-31+G(d,p) basis set. Spin-unrestricted calculations (UB3LYP) were used for open-shell systems. Spin contamination in the UB3LYP calculation was small as judged from the $\langle S^2 \rangle$ operator expectation values that were 0.75−0.77. The optimized structures were characterized by harmonic frequency analysis as local minima (all frequencies real) or first-order saddle points (one imaginary frequency). Complete optimized structures in the Cartesian coordinate format are available as Supporting Information. The B3LYP/6-31+G(d,p) frequencies were scaled by 0.963 (ref 28, for other scaling factors see ref 29) and used to calculate zero-point vibrational energies (ZPVE), enthalpy corrections, and partition functions. Single-point energies were calculated at several levels of theory. In one set of calculations, MP2(frozen core)[30] and B3LYP energies were calculated with the larger 6-311+G(2df,p) basis set. Spin contamination in the UMP2 calculations was substantial for the nitrobenzene radicals and transition states, as evidenced by the spin expectation values $\langle S^2 \rangle$ that ranged between 1.1 and 1.6. Spin annihilation using Schlegel's projection method[31] (PMP2)[26] reduced the $\langle S^2 \rangle$ values to 0.77−0.88 for local minima and 1.1−1.5 for transition states. In addition, restricted open-shell (ROMP2) calculations[32] were carried out for the entire set of structures to deal with the spin contamination problem.[33] The PMP2 and ROMP2 energies were averaged with the B3LYP energies according to the empirical procedure that was introduced previously[34] and tested for several systems since.[35,36] This resulted in error cancellation and provided excellent relative energies, denoted as B3-PMP2 or B3-ROMP2,[36] as discussed below. Calculations on closed-shell systems are marked by B3-MP2. In addition, a composite procedure was adopted that consisted of a single-point quadratic configuration interaction calculation,[37] QCISD(T)/6-31G(d,p), and basis set expansion up to 6-311+G(3df,2p) through PMP2 or ROMP2 single-point calculations according to eq 1:

$$\text{QCISD(T)/6-311+G(3df,2p)} \approx \text{QCISD(T)/6-31G(d,p)} + \text{MP2/6-311+G(3df,2p)} - \text{MP2/6-31G(d,p)} \quad (1)$$

This level of theory is intermediate between those of the Gaussian 2 (MP2) method[38] which uses the 6-311G(d,p) basis set in the large QCISD(T) calculation and the G2(MP2, SVP) method[39] which uses the 6-31G(d) basis set instead. We also utilized the previous finding that restricted open-shell calculations (ROMP2) provided good stabilization energies for small organic radicals.[33] A basis set expansion to effective QCISD(T)/6-311+G(2df,p) was also tested for selected systems. The calculated total energies are available as Supporting Information. The relative energies are presented in Tables 1−7.

Franck−Condon energies in vertical neutralization and reionization were taken as absolute differences between the total B3LYP/6-311+G(2df,p) energies of fully optimized ion or neutral structures and those in which an electron has been added to an optimized cation structure

(23) Turecek, F. *Org. Mass Spectrom.* **1992**, *27*, 1087.

(24) (a) Høg, J. H. *J. Label. Comput.* **1971**, *7*, 179. (b) Alexander, E. R.; Burge, R. E. *J. Am. Chem. Soc.* **1950**, *72*, 3100. (c) Murray, A.; Williams, D. L. *Organic Syntheses with Isotopes*; Wiley-Interscience: New York, 1958; pp 1375 and 1592.

(25) Black, A. P.; Babers, F. H. *Org. Synth.* **1939**, *19*, 64.

(26) Frisch, M. J.; Trucks, G. W.; Schlegel, H. B.; Scuseria, G. E.; Robb, M. A.; Cheeseman, J. R.; Zakrzewski, V. G.; Montgomery, J. A., Jr.; Stratmann, R. E.; Burant, J. C.; Dapprich, S.; Millam, J. M.; Daniels, A. D.; Kudin, K. N.; Strain, M. C.; Farkas, O.; Tomasi, J.; Barone, V.; Cossi, M.; Cammi, R.; Mennucci, B.; Pomelli, C.; Adamo, C.; Clifford, S.; Ochterski, J.; Petersson, G. A.; Ayala, P. Y.; Cui, Q.; Morokuma, K.; Malick, D. K.; Rabuck, A. D.; Raghavachari, K.; Foresman, J. B.; Cioslowski, J.; Ortiz, J. V.; Stefanov, B. B.; Liu, G.; Liashenko, A.; Piskorz, P.; Komaromi, I.; Gomperts, R.; Martin, R. L.; Fox, D. J.; Keith, T.; Al-Laham, M. A.; Peng, C. Y.; Nanayakkara, A.; Gonzalez, C.; Challacombe, M.; Gill, P. M. W.; Johnson, B. G.; Chen, W.; Wong, M. W.; Andres, J. L.; Head-Gordon, M.; Replogle, E. S.; Pople, J. A. *Gaussian 98*, revision A.6; Gaussian, Inc.: Pittsburgh, PA, 1998.

(27) (a) Becke, A. D. *J. Chem. Phys.* **1993**, *98*, 1372 and 5648. (b) Stephens, P. J.; Devlin, F. J.; Chablowski, C. F.; Frisch, M. J. *J. Phys. Chem.* **1994**, *98*, 11623.

(28) (a) Rauhut, G.; Pulay, P. *J. Phys. Chem.* **1995**, *99*, 3093. (b) Finley, J. W.; Stephens, P. J. *J. Mol. Struct. (THEOCHEM)* **1995**, *227*, 357. (c) Wong, M. W. *Chem. Phys. Lett.* **1996**, *256*, 391.

(29) Scott, A. P.; Radom, L. *J. Phys. Chem.* **1996**, *100*, 16502.

(30) Møller, C.; Plesset, M. S. *Phys. Rev.* **1934**, *46*, 618.

(31) (a) Schlegel, H. B. *J. Chem. Phys.* **1986**, *84*, 4530. (b) Mayer, I. *Adv. Quantum Chem.* **1980**, *12*, 189.

(32) McWeeny, R.; Diercksen, G. *J. Chem. Phys.* **1968**, *49*, 4852.

(33) Parkinson, C. J.; Mayer, P. M.; Radom, L. *J. Chem. Soc., Perkin Trans. 2*, **1999**, 2305.

(34) Turecek, F. *J. Phys. Chem. A*, **1998**, *102*, 4703.

(35) (a) Turecek, F.; Wolken, J. K. *J. Phys. Chem. A*, **1999**, *103*, 1905. (b) Wolken, J. K.; Turecek, F. *J. Phys. Chem. A*, **1999**, *103*, 6268. (c) Wolken, J. K.; Turecek, F. *J. Am. Chem. Soc.* **1999**, *121*, 6010. (d) Turecek, F.; Carpenter, F. H. *J. Chem. Soc., Perkin Trans. 2* **1999**, 2315. (e) Turecek, F.; Polasek, M.; Frank, A. J.; Sadilek, M. *J. Am. Chem. Soc.* **2000**, *122*, 2361.

(36) Rablen, P. R. *J. Am. Chem. Soc.* **2000**, *122*, 357.

(37) Pople, J. A.; Head-Gordon, M.; Raghavachari, K. *J. Chem. Phys.* **1987**, *87*, 5968.

(38) (a) Curtiss, L. A.; Raghavachari, K.; Pople, J. A. *J. Chem. Phys.* **1993**, *98*, 1293.

(39) (a) Curtiss, L. A.; Redfern, P. C.; Smith, B. J.; Radom, L. *J. Chem. Phys.* **1996**, *104*, 5148. (b) Smith, B. J.; Radom, L. *J. Phys. Chem.* **1995**, *99*, 6468.

Table 1. Dissociation Energies of Ions

	reaction enthalpy[a−c]									
method	**1**	**2**	**3**	**4**	**5**	**6**	**7**	**8**	**9**	rmsd
B3LYP/6-31+G(d,p)	814	442	227	264	262	293	−154	140	234	22
B3LYP/6-311+G(2df,p)	814	440	229	261	259	269	−128	131	229	16
PMP2/6-311+G(2df,p)		439	289					139	224	41
ROMP2/6-311+G(2df,p)	784	433	298	300	298	203	−46	146	212	41
PMP2/6-311+G(3df,2p)		*d*	285					*d*	224	
ROMP2/6-311+G(3df,2p)	786	436	300	300	299	207	−50	149	213	41
B3-PMP2/6-311+G(2df,p)		440	259					135	226	19
B3-ROMP2/6-311+G(2df,p)	799	436	263	281	279	236	−87	138	221	21
exp.	800	443	223		259	243		144	242	

[a] Including B3LYP/6-31+G(d,p) zero-point corrections and 298 K enthalpy corrections. [b] In kJ mol^{-1}. [c] Reaction 1: $C_6H_5NO_2H^+ \rightarrow C_6H_5NO_2 + H^+$. Reaction 2: $C_6H_5NO_2H^+ \rightarrow C_6H_5NO_2^{+\bullet} + H^\bullet$. Reaction 3: $C_6H_5NO_2H^+ \rightarrow C_6H_5NO^{+\bullet} + OH^\bullet$. Reaction 4: $C_6H_5NO_2H^+ \rightarrow C_6H_5^+ +$ *syn*-HONO. Reaction 5: $C_6H_5NO_2H^+ \rightarrow C_6H_5^+ +$ *anti*-HONO. Reaction 6: $C_6H_5NO_2H^+ \rightarrow C_6H_6 + NO_2^+$. Reaction 7: $C_6H_6 + NO_2^+ \rightarrow$ *ipso*-$C_6H_6NO_2^+$ (**5**$^+$). Reaction 8: $C_6H_5NO_2^{+\bullet} \rightarrow C_6H_5^+ + NO_2$. Reaction 9: $C_6H_5NO^{+\bullet} \rightarrow C_6H_5^+ +$ NO. [d] The UHF calculations did not converge.

or subtracted from an optimized neutral structure. No zero-point corrections were applied to the calculated Franck−Condon energies. Excited-state energies were obtained from single-point calculations using the complete active space (CASSCF)[40] method with the 6-31G-(d,p) basis set. Oscillator strengths were calculated with the configuration-interaction singles (CIS) method[41] and the 6-311+G(2df,p) basis set.

RRKM calculations used Hase's program[42] that was recompiled for MS-DOS and run under Windows NT.[43] Vibrational state densities were obtained by direct count of quantum states in 2 kJ mol^{-1} steps for internal energies up to 80−120 kJ mol^{-1} above the threshold. The rotational states were treated adiabatically[44] and the microscopic rate constants, *k(E,J,K)*, were Boltzmann-averaged over the thermal distribution of rotational *J* and *K* states pertaining to the ion source temperature. Thermal rate constants were calculated using the standard transition state theory formulas.[45] The activation energies were taken from single-point calculations, the partition functions were calculated from the B3LYP/6-31+G(d,p) moments of inertia and scaled harmonic frequencies using the rigid rotor-harmonic oscillator approximation.

Results and Discussion

Phenylnitronic Radical (1). Radical **1** was generated by selective protonation of nitrobenzene followed by collisional electron transfer (Scheme 2). The topical proton affinities (PA) in nitrobenzene were calculated previously at an intermediate level of theory and found to greatly prefer protonation at an oxygen atom of the nitro group for which PA = 813 kJ mol^{-1} was calculated[46] in fair agreement with the experimental PA of nitrobenzene (800 kJ mol^{-1}).[47] The B3-MP2 proton affinity for protonation at the nitro group calculated in the present work, PA = 799 kJ mol^{-1}, was in excellent agreement with the tabulated value (Table 1, reaction 1). The topical PA of the *ipso*, *ortho*, and *meta* positions in nitrobenzene were calculated to be substantially lower,for example, 650, 676, and 676 kJ mol^{-1}, respectively, according to B3-MP2 calculations which agreed within 10 kJ mol^{-1} with the previous computational data.[46] The topical proton affinities of the *para* and *ortho* positions are very similar[46] and so the former datum has not been reexamined here. Gas-phase protonation with $CH_3C{=}NH^+$ (PA(CH_3CN) = 779 kJ mol^{-1}, ref [47]) was therefore energetically possible to occur only in the nitro group to form ion **1**$^+$. Likewise, gas-phase deuteronation with $CD_3C{=}ND^+$ introduced the deuteron in the nitro group to form ion **1a**$^+$. Ions **1**$^+$ and **1a**$^+$ were characterized by collisionally activated dissociation spectra;[48] that of **1**$^+$ was in qualitative agreement with the previous measurements of Crombie and Harrison.[49]

Collisional neutralization of stable **1**$^+$ and its isotopomers gave rise to radicals **1**, **1a** and **1e** that were characterized by NR mass spectra (Figure 1a−c). NRMS of **1** showed a prominent survivor ion at *m/z* 124 as evidence that a substantial fraction of **1** did not dissociate on the 5.3 μs time scale. The NR dissociations that were observed resulted in the formation of $C_6H_5NO_2$ (*m/z* 123, loss of H), C_6H_5NO (*m/z* 107, loss of OH), C_6H_6O (*m/z* 94, loss of NO), C_6H_5 (*m/z* 77, loss of HONO), NO (*m/z* 30), and aromatic hydrocarbon fragments at *m/z* 73−76, 62−65, 49−51, 36−39, and 24−26. These dissociations could occur from the intermediate radical **1** and/or following collisional reionization to **1**$^+$.[50] Note that the CAD spectrum of **1**$^+$ (ref 48) showed qualitatively the same fragments as did the NR spectrum. Hence, the neutral and post-reionization dissociations needed to be resolved. The stability under NR conditions of the presumed neutral intermediates was investigated for nitrobenzene, nitrosobenzene and the phenyl radical (Figure 2a−c). Phenol, another possible intermediate, is known to be stable in NRMS.[23,51] Nitrobenzene showed a moderately abundant survivor ion and fragments formed by loss of NO_2 and subsequent ring cleavages of neutral or ionic C_6H_5 (Figure 2a). The NR mass spectrum of $C_6H_5NO_2$ was remarkably similar to the recent photofragmentation spectrum obtained with 90 fs laser pulses in which both neutral and ion dissociations were considered.[52] NRMS of nitrosobenzene resulted in substantial dissociation to C_6H_5 and NO so that only a weak survivor ion

(40) (a) Hegarty, D.; Robb, M. A. *Mol. Phys.* **1979**, *38*, 1795. (b) Eade, R. H. E.; Robb, M. A. *Chem. Phys. Lett.* **1981**, *83*, 362.
(41) Foresman, J. B.; Head-Gordon, M.; Pople, J. A.; Frisch, M. J. *J. Phys. Chem.* **1992**, *96*, 135.
(42) Zhu, L.; Hase, W. L. *Quantum Chemistry Program Exchange*; Indiana University: Bloomington, IN, 1994; Program No. QCPE 644.
(43) Frank, A. J.; Sadilek, M.; Ferrier, J. G.; Turecek, F. *J. Am. Chem. Soc.* **1997**, *119*, 12343.
(44) Zhu, L.; Hase, W. L. *Chem. Phys. Lett.* **1990**, *175*, 117.
(45) Levine, I. N. *Physical Chemistry*, 3rd ed.; McGraw-Hill: New York, 1988; p 839.
(46) Eckert-Maksic, M.; Hodoscek, M.; Kovacek, D.; Maksic, Z. B.; Primorac, M. *J. Mol. Struct. (THEOCHEM)* **1997**, *417*, 131.
(47) *NIST Standard Reference Database No. 69*, February 2000 Release. http://webbook.nist.gov/chemistry.
(48) The CAD spectra of **1**$^+$ and **1a**$^+$ were as follows: **1**$^+$ (*m/z*, rel intens) 26(0.3), 27(0.5), 30(0.7), 36(0.4), 37(0.9), 38(1.2), 39(1.4), 48(0.2), 49-(0.9), 50(7.2), 51(9.7), 52(0.5), 60(0.2), 61(0.5), 61.5(0.2), 62(3.2), 63(1.1), 64(0.7), 65(2.4), 66(0.7), 73(0.4), 74(2.2), 75(2.2), 76(8.2), 77(34.0), 78-(4.0), 91(0.2), 93(1.2), 94(6.5), 106(0.2), 107(4.8), 123(2.6). **1a**$^+$ (*m/z*, rel intens) 24(0.2), 26(0.4), 27(0.4), 30(0.7), 36(0.4), 37(1.2), 38(1.1), 39(0.9), 40(0.4), 41(0.3), 42(0.3), 44(0.2), 48(0.2), 49(0.8), 50(6.6), 51(8.7), 52-(0.70), 54(0.4), 60(0.5), 61(0.5), 62(0.9), 62.5(2.9), 63(1.0), 64(0.9), 65-(0.6), 66(1.0), 67(0.6), 73(0.5), 74(1.9), 75(1.7), 76(7.9), 77(31.1), 78(2.6), 79(2.0), 91(0.3), 94(0.5), 95(6.9), 106(0.4), 107(5.4), 123(0.3), 124(2.9).
(49) Crombie, R. A.; Harrison, A. G. *Org. Mass Spectrom.* **1988**, *23*, 327.
(50) Abboud, J. L. M.; Notario, R.; Yanez, M.; Mo, O.; Flammang, R.; Jagerovic, N.; Alkorta, I.; Elguero, J. *J. Phys. Org. Chem.* **1999**, *12*, 787.
(51) Turecek, F.; Drinkwater, D. E.; Maquestiau, A.; McLafferty, F. W.; *Org. Mass Spectrom.* **1989**, *24*, 669.

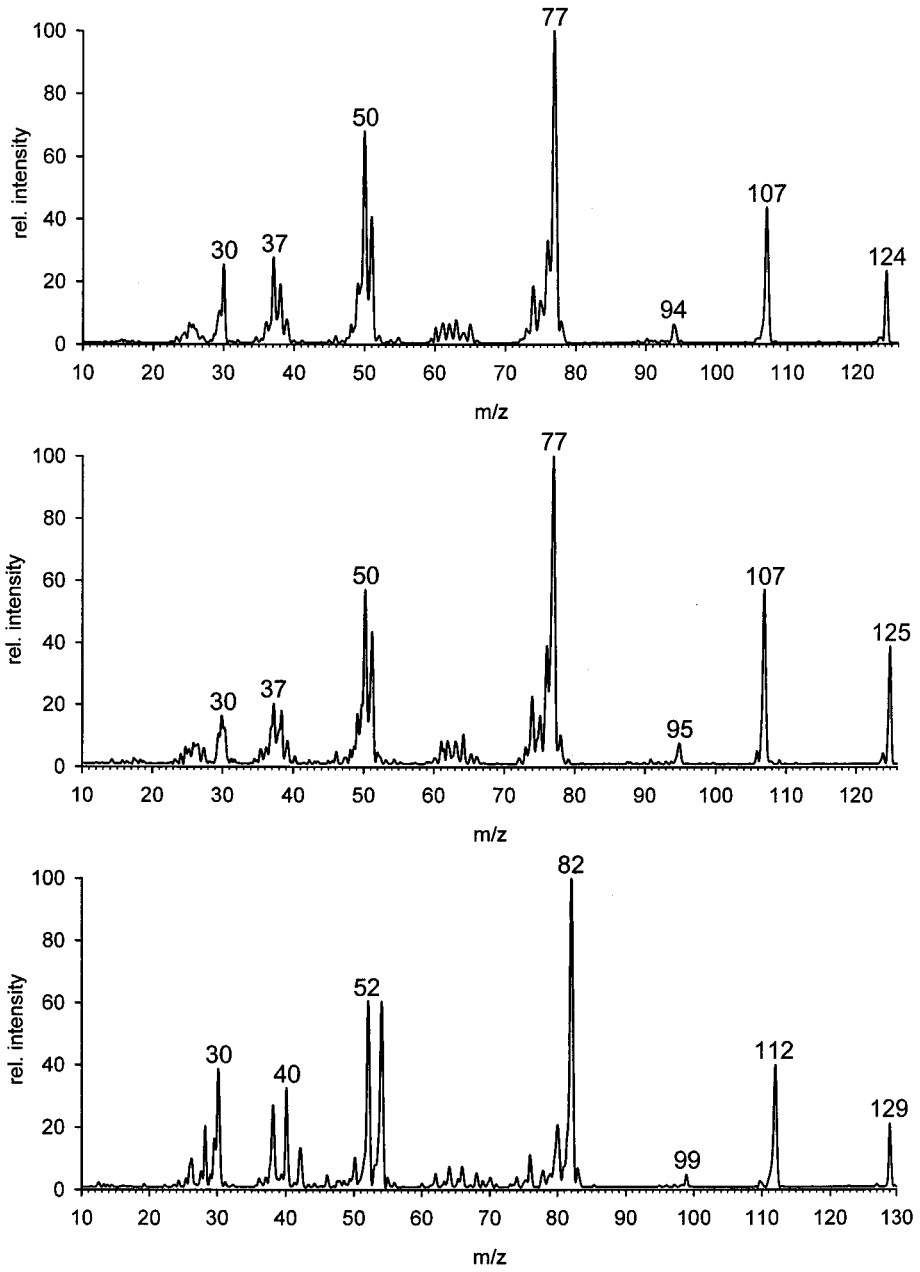

Figure 1. Neutralization (CH_3SSCH_3, 70%T)−reionization (O_2, 70%T) spectra of (a) $\mathbf{1}^+$, (b) $\mathbf{1a}^+$, and (c) $\mathbf{1e}^+$.

was found (Figure 2b). NRMS of $C_6H_5^+$ showed an abundant survivor ion and dissociations by hydrogen atom losses and ring fragmentations (Figure 2c).

Deuterium labeling in the nitro group revealed clean losses of H (but not D!), OD, and DONO from **1a** upon NR (Figure 1b). These were confirmed by the NR mass spectrum of the complementarily labeled D_5-ion ($\mathbf{1e}^+$) which showed clean losses of D, OH, and HONO (Figure 1c). Deuterium labeling thus proved that the hydroxyl hydrogen atom did not exchange with the ring hydrogens in stable radicals **1** nor in the course of radical and/or post-reionization dissociations. The intriguing loss of hydrogen atom was further studied with radicals **1b**−**d** produced from specifically labeled ions $\mathbf{1b}-\mathbf{d}^+$. The relative intensities of NR ions formed by loss of H and D, denoted as [**1b** − H], [**1b** − D], etc., were fitted into mass-balance homogeneous linear equations (eq 2−4)

$$\frac{k_D/k_H[\text{ortho}]}{[\text{ortho}]+2[\text{meta}]+[\text{para}]}=\frac{[\mathbf{1b}-\text{D}]}{[\mathbf{1b}-\text{H}]}=0 \quad (2)$$

$$\frac{k_D/k_H[\text{meta}]}{2[\text{ortho}]+2[\text{meta}]+[\text{para}]}=\frac{[\mathbf{1c}-\text{D}]}{[\mathbf{1c}-\text{H}]}=0.079 \quad (3)$$

$$\frac{k_D/k_H[\text{para}]}{2[\text{ortho}]+2[\text{meta}]}=\frac{[\mathbf{1d}-\text{D}]}{[\mathbf{1d}-\text{H}]}=0.079 \quad (4)$$

to obtain the fractional losses from the *ortho*, *meta*, and *para* positions marked as [ortho], [meta], and [para]. The best fit was obtained when considering an average kinetic isotope effect for the cleavage of the C−H bond as $k_H/k_D = 3.05$. The fractions favored loss of H from the *para* position (61%) and both *meta* positions (39% total) in $\mathbf{1}^+$, whereas the hydrogen atoms in the *ortho* positions and the NO_2H group were unreactive. Similar fractions for the losses from $\mathbf{1}^+$ of the *ortho*, *meta*, and *para*

(52) (a) Kosmidis, C.; Ledingham, K. W. D.; Kilic, H. S.; McCanny, T.; Singhal, R. P.; Langley, A. J.; Shaikh, W. *J. Phys. Chem.* **1997**, *101*, 2264. For other photodissociation studies, see: (b) Galloway, D. B.; Bartz, J. A.; Huey, L. G.; Crim, F. F. *J. Chem. Phys.* **1993**, *98*, 2107. (c) Kosmidis, C.; Ledingham, K. W. D.; Clark, A.; Marshall, A.; Jennings, R.; Sander, J.; Singhal, R. P. *Int. J. Mass Spectrom. Ion Processes* **1994**, *135*, 229.

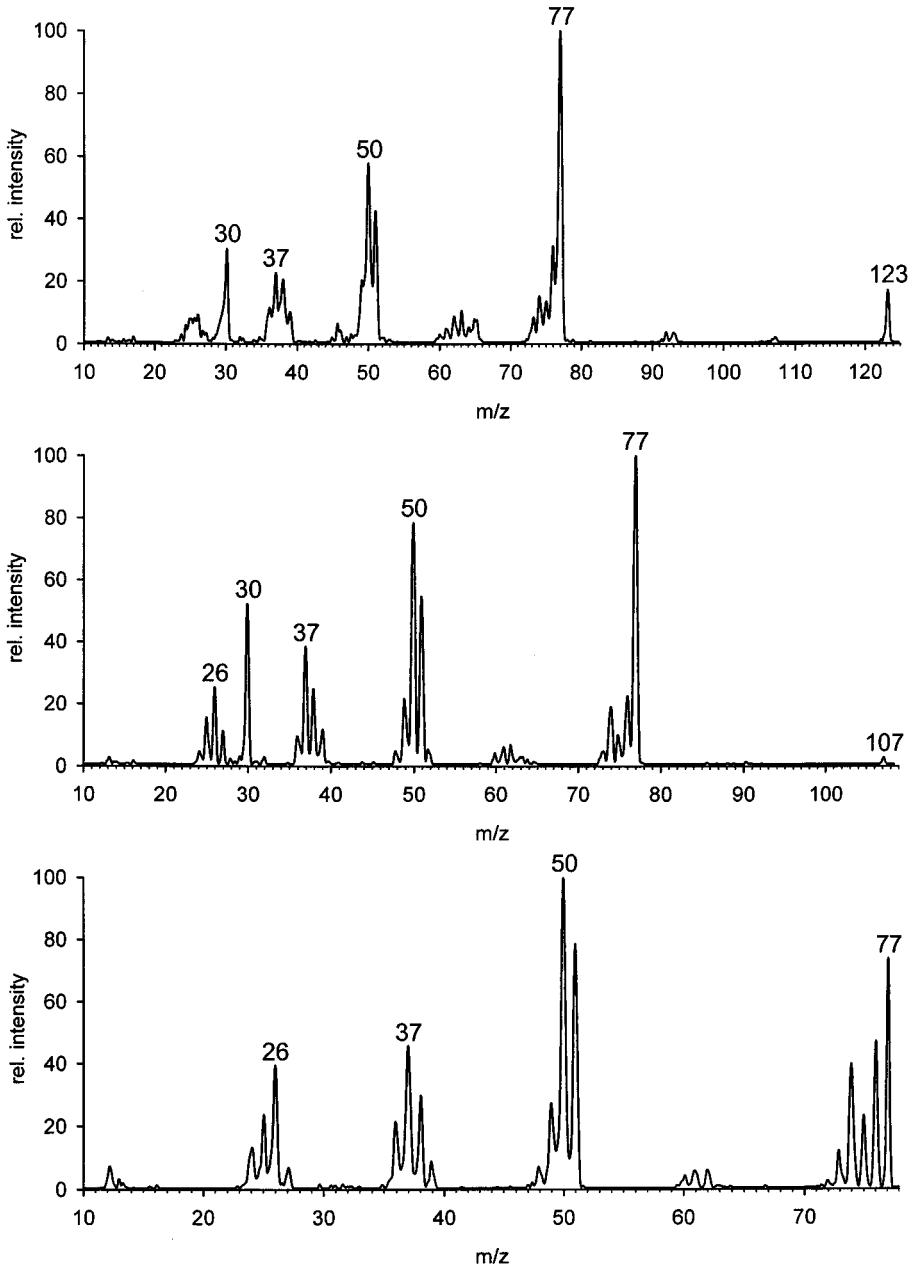

Figure 2. Neutralization (CH_3SSCH_3, 70%T)−reionization (O_2, 70%T) spectra of (a) nitrobenzene$^{+\bullet}$, (b) nitrosobenzene$^{+\bullet}$, and (c) $C_6H_5^+$.

hydrogen atoms were obtained from analysis of CAD spectra. The absence of loss of H from the NO_2H group showed that nitrobenzene was not formed from **1**, nor was its cation-radical formed from $\mathbf{1}^{+\bullet}$.[53] Radicals **1**, **1a**, and **1e** were also generated from the corresponding ions prepared by highly exothermic protonation of nitrobenzene with CH_5^+ or CD_5^+. Comparison of the proton affinity of CH_4 (543 kJ mol^{-1})[47] with the topical proton affinities of the ring positions in nitrobenzene (vide supra) indicated that ring protonation with CH_5^+ was >100 kJ mol^{-1} exothermic and therefore energetically possible for each position. However, the NR mass spectra of [nitrobenzene + H]$^+$ and [nitrobenzene + D]$^+$ ions from protonation with CH_5^+ or CD_5^+ (spectra not shown) were very similar to those of $\mathbf{1}^+$, $\mathbf{1a}^+$, and $\mathbf{1e}^+$, respectively. In particular, losses of OH or OD, and HONO or DONO cleanly incorporated the proton or deuteron previously introduced by the gas-phase acid. This ruled out participation of Wheland structures **2**−**4** which would contain chemically equivalent geminal H and D atoms that should be transferred to the nitro group with similar probabilities when allowing for isotope effects. Wheland radical **5** was expected to competitively eliminate the *ipso* hydrogen atom and the NO_2 group (vide infra). However, neither of these dissociations was enhanced in the NR spectrum of [nitrobenzene + D]$^+$ from deuteronation with CD_5^+. Hence it follows that Wheland ion structures $\mathbf{2}^+$−$\mathbf{5}^+$ *were not present* in the ion population formed by the highly exothermic protonation of nitrobenzene.

The reason for this observation can be 2-fold. First, the ion−molecule reaction of nitrobenzene with CH_5^+ requires formation of an ion−dipole complex which should slightly favor CH_5^+ interaction with the negatively charged oxygen atoms of the nitrobenzene dipole. However, an upper-limit estimate from the locked-dipole theory[54] indicated <1% increase of reaction rate due to locked ion−dipole interaction favoring protonation at the nitro group.[55] Second, even if Wheland structures were

(53) Polasek, M.; Turecek, F.; Flammang, R.; Gerbaux, P. Unpublished results.

(54) (a) Moran, T. F.; Hamill, W. H. *J. Chem. Phys.* **1963**, *39*, 1413. (b) Theard, L. P.; Hamill, W. H. *J. Am. Chem. Soc.* **1962**, *84*, 1134.

Table 2. Anion Energies

reaction	energy[a] B3LYP/6-31+G(d,p)	B3LYP/6-311+G(2df,p)	PMP2/6-311+G(2df,p)	B3−PMP2
$C_6H_5NO_2 + H^- \rightarrow C_6H_5NO_2H^-$ (**1**$^-$)	−423	−291	−301	−296
$C_6H_5NO_2 + H^- \rightarrow$ *ortho*-H−$C_6H_5NO_2$- (**2**$^-$)	−433	−303	−314	−309
$C_6H_5NO_2 + H^- \rightarrow$ *meta*-H−$C_6H_5NO_2$- (**3**$^-$)	−332	−205	−242	−224
$C_6H_5NO_2 + H^- \rightarrow$ *para*-H−$C_6H_5NO_2$- (**4**$^-$)	−434	−305	−314	−310
1$^-$ + $C_6H_5NO_2 \rightarrow C_6H_5NO_2^{-\bullet}$ + **1**	−5	−6	38	16
2$^-$ + $C_6H_5NO_2 \rightarrow C_6H_5NO_2^{-\bullet}$ + **2**	55	6	51	29
3$^-$ + $C_6H_5NO_2 \rightarrow C_6H_5NO_2^{-\bullet}$ + **3**	−96	−92	−21	−56
4$^-$ + $C_6H_5NO_2 \rightarrow C_6H_5NO_2^{-\bullet}$ + **4**	7	9	51	30
$C_6H_5NO_2^{-\bullet} \rightarrow C_6H_5NO_2$	124 (1.29)[b]	121 (1.25)[b]	69.5 (0.72)[b]	95 (0.99)[b]
$C_6H_5NO_2H^-$ (**1**$^-$) → **1**	119 (1.24)	115 (1.19)	108 (1.11)	111 (1.15)
ortho-H−$C_6H_5NO_2$- (**2**$^-$) → **2**	204 (2.12)	204 (2.11)	193 (2.00)	199 (2.06)
meta-H−$C_6H_5NO_2$- (**3**$^-$) → **3**	127 (1.32)	128 (1.33)	146 (1.51)	137 (1.42)
para-H−$C_6H_5NO_2$- (**4**$^-$) → **4**	208 (2.16)	208 (2.16)	199 (2.06)	203 (2.11)

[a] In units of kJ mol^{-1} at 298 K. [b]Electron affinities in eV.

formed by exothermic protonation, they could be depleted by exothermic proton transfer to neutral nitrobenzene producing **1**$^+$. Under standard chemical ionization conditions, neutral nitrobenzene is the second most abundant species in the ion source (after the CI reagent gas), and secondary reactions of it with high-energy [nitrobenzene + H]$^+$ ions cannot be avoided. Note that *intramolecular* isomerization of **2**$^+$−**5**$^+$ to the much more stable **1**$^+$ would result in hydrogen scrambling which was ruled out by the labeling experiments.

Other attempts at generating ion precursors of **2**−**5** were unsuccessful. Gas-phase nitration of benzene with the $CH_3OH-NO_2^+$ complex was reported to produce the ipso ion **5**$^+$ as a reaction intermediate.[56] We performed ion−molecule reactions of $CH_3OH-NO_2^+$ with benzene and C_6D_6 that afforded abundant nitration products at *m*/*z* 124 and *m*/*z* 130, respectively. However, the NR mass spectra of the *m*/*z* 124 and *m*/*z* 130 ions were identical to those of **1**$^+$ and **1e**$^+$, respectively. In particular, the NR spectra of the *m*/*z* 124 and *m*/*z* 130 ions from gas-phase nitration showed negligible C_6H_6 and C_6D_6 product intensities that would have been indicative of the presence of **5** or its deuterium-labeled derivative (vide infra). This strongly indicated that ion **5**$^+$ rearranged rapidly to the more stable isomer **1**$^+$, as postulated previously.[56] Rearrangement to **1e**$^+$ of the ionic Wheland intermediate $C_6D_6-NO_2^+$ was also indicated by gas-phase H/D exchange with methanol that produced $C_6D_5NO_2H^+$ at *m*/*z* 129.

Addition of H$^-$ to nitrobenzene was predicted by B3-MP2 calculations to be exothermic when forming anions **1**$^-$−**4**$^-$ (Table 2). By comparison, the B3-MP2 calculated electron affinity of nitrobenzene (0.99 eV, Table 2) was close to the experimental value (1.00−1.01 eV).[47] Despite the favorable thermochemistry of hydride additions to nitrobenzene, ion−molecule reactions of H$^-$ with $C_6H_5NO_2$ and $C_6D_5NO_2$ yielded only the corresponding nitrobenzene anion-radicals at *m*/*z* 123 and 128, respectively. This result was independent of the mode of H$^-$ generation by either dissociative electron capture in H_2 (ref 57) or hydride transfer from CH_3O^- (ref 58). Interestingly, anions **1**$^-$− **4**$^-$ were found to be substantially stable with respect to hydrogen atom elimination to form $C_6H_5NO_2^{-\bullet}$, as judged from the calculated reaction enthalpies (Table 2). However, hydrogen transfer reactions to nitrobenzene were calculated to be energetically possible and can provide a mechanism for depletion of ions **1**$^-$− **4**$^-$ (Table 2). Potential energy barriers can be another factor hampering hydride additions to nitrobenzene, but these were not studied in this work.

The dissociations of neutral **1** and post-reionization dissociations of **1**$^+$ were distinguished by variable-time measurements. These yielded phenomenological rate parameters that were used to quantify the contributions of neutral (k_N) and ion (k_i) processes to dissociations observed upon NR. Two dissociations were investigated: Loss of OH was monitored in the $C_6H_5NO^{+\bullet}$ channel, and loss of HONO was monitored in the $C_6H_5^+$ channel. Unfortunately, ions from the complementary neutral fragments, OH and HONO, respectively, were too weak to be measured reliably.[59] The rate parameters indicated participation of both neutral and ion dissociations, for example, $k_N(C_6H_5NO) = (2.8 \pm 0.1) \times 10^5$ s^{-1}, $k_i(C_6H_5NO^{+\bullet}) = (4.0 \pm 0.1) \times 10^5$ s^{-1}, and $k_N(C_6H_5) = (4.8 \pm 0.1) \times 10^5$ s^{-1}, $k_i(C_6H_5^+) = (9.0 \pm 0.1) \times 10^5$ s^{-1}. However, variable-time measurements also showed that C_6H_5NO, when prepared by collisional neutralization, underwent both neutral and ion dissociations by loss of NO to form $C_6H_5^\bullet$ and $C_6H_5^+$, respectively. The rate parameters for unimolecular NR dissociations of C_6H_5NO were substantial, that is, $k_N(C_6H_5) = (7.4 \pm 0.5) \times 10^5$ s^{-1}, $k_N(NO) = (8.2 \pm 0.5) \times 10^5$ s^{-1}, $k_i(C_6H_5^+) = (7.3 \pm 0.5) \times 10^5$ s^{-1}, and $k_i(NO^+) = (1.2 \pm 0.1) \times 10^6$ s^{-1}. Hence, the formation of C_6H_5 (radical or ion) can be due to *consecutive dissociations* of nitrosobenzene produced as a primary product from **1**. To distinguish the direct and consecutive dissociations of **1** we resorted to ab initio and density functional calculations that furnished activation energies and rate constants.

Radical and Ion Energetics. Geometry optimizations with B3LYP/6-31+G(d,p) found local energy minima for **1**−**5** (Figure 3) as confirmed by harmonic frequency analysis. Interestingly, only the planar *syn* rotamer of **1** of C_s symmetry was a stable structure, while the quasiplanar *anti* isomer was a transition state for internal rotation of the OH group (**TS11**, Figure 3). Wheland adducts **2**−**4** showed unexceptional bond lengths and angles. The *ipso* isomer **5** had a long C_{ipso}−N bond (1.610 Å) that indicated facile dissociation (vide infra). At all

(55) Calculated by using the tabulated values for the dipole moment, $\mu_D = 4.22$ D, and polarizability, $a = 12.9-14.7 \times 10^{-24}$ cm^3, of nitrobenzene. See: Lide, D. H. *CRC Handbook of Chemistry and Physics*, 71st ed.; CRC Press: Boca Raton, FL, 1990.

(56) (a) Attina, M.; Cacace, F.; Speranza, M. *Int. J. Mass Spectrom. Ion Processes* **1992**, *117*, 37. (b) Aschi, M.; Attina, M.; Cacace, F.; Ricci, A. *J. Am. Chem. Soc.* **1994**, *116*, 9535. (c) Attina, M.; Cacace, F.; Ricci, A. *J. Phys. Chem.* **1996**, *100*, 4424.

(57) Budzikiewicz, H. *Mass Spectrom. Rev.* **1986**, *5*, 345.

(58) (a) Ingemann, S.; Kleingeld, J. C.; Nibbering, N. M. M. *J. Chem. Soc., Chem. Commun.* **1982**, 1009. (b) Nibbering, N. M. M. *Adv. Phys. Org. Chem.* **1988**, *24*, 1−55.

(59) Vertical ionization of HONO is accompanied by large Franck−Condon effects that result in facile ion dissociation, see: Polasek, M.; Turecek, F. *J. Phys. Chem. A*, **1999**, *103*, 9241. OH has a substantially smaller ionization cross section than C_6H_5NO.

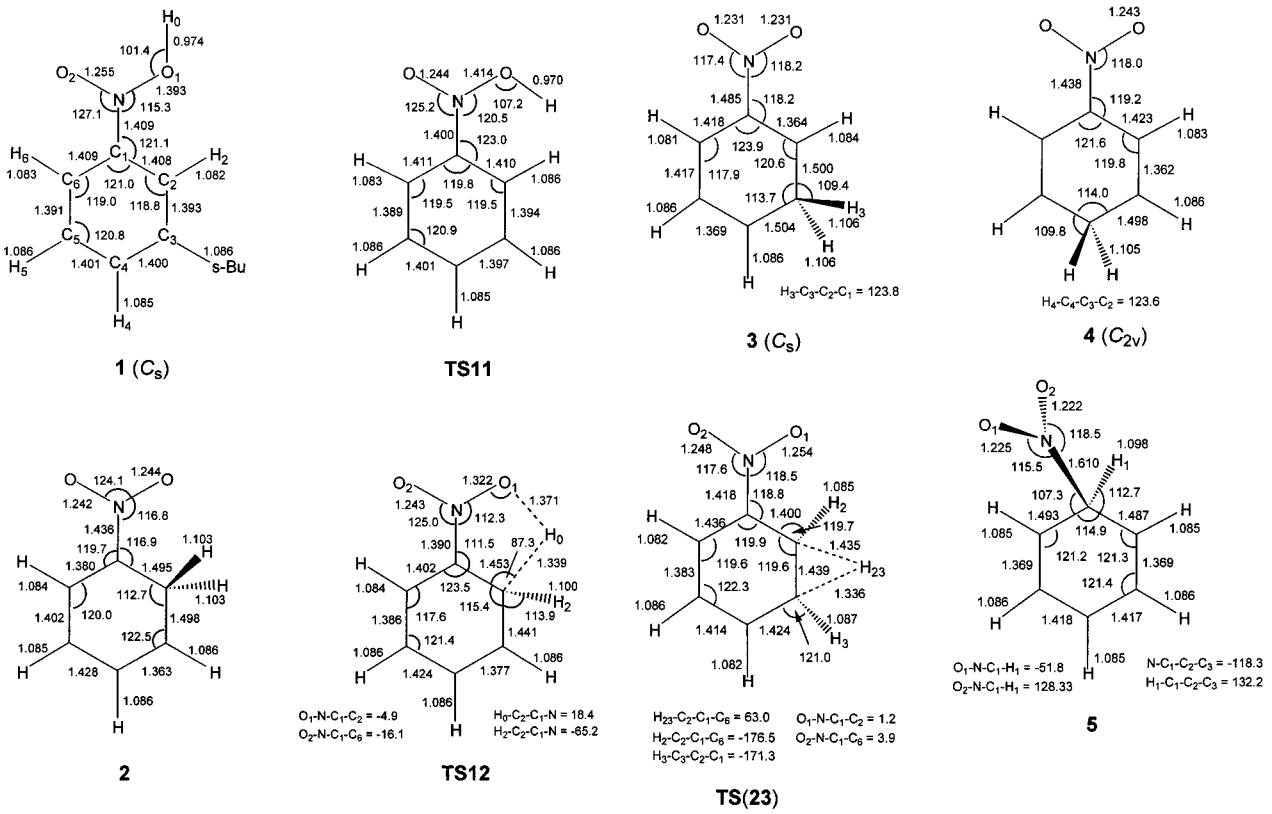

Figure 3. B3LYP/6-31+G(d,p)-optimized structures of **1**−**5** and transition states. Bond lengths in Å, bond and dihedral angles in degrees.

Table 3. Relative Energies of Nitrobenzene Radicals

	relative enthalpy[a,b]				
method	**1**	**2**	**3**	**4**	**5**
B3LYP/6-31+G(d,p)	0	75	99	78	104
B3LYP/6-311+G(2df,p)	0	77	99	79	104
PMP2/6-311+G(2df,p)	0	67	82	71	87
ROMP2/6-311+G(2df,p)	0	73	97	78	98
PMP2/6-311+G(3df,2p)	0	66	83	71	86
ROMP2/6-311+G(3df,2p)	0	72	98	78	97
QCISD(T)/6-311+G(2df,p)					
UMP2	0	67	81	67	81
PMP2	0	65	79	66	81
ROMP2	0	66	81	69	83
QCISD(T)/6-311+G(3df,2p)					
UMP2	0	66	81	67	80
PMP2	0	65	80	66	80
ROMP2	0	65	81	69	82
B3-PMP2/6-311+G(2df,p)	0	72	91	75	95
B3-ROMP2/6-311+G(2df,p)	0	75	98	78	101
	0[c]	76[c]	99[c]	80[c]	102[c]

[a] Including B3LYP/6-31+G(d,p) zero-point and 298 K enthalpy corrections. [b] In kJ mol^{-1}. [c] 0 K values.

levels of theory, **1** was the most stable isomer, followed by the *ortho*, *para*, *meta*, and *ipso* Wheland adducts (Table 3).

To judge the quality of the relative energies calculated at various levels of theory, we obtained 298 K enthalpies for dissociations and ionization of nitrobenzene and nitrosobenzene, for which there are experimental thermochemical data.[47] Likewise, ion dissociation energies were calculated and compared with values that were derived from experimental enthalpies of formation. The results are summarized in Tables 1 and 4. The neutral dissociation energies were approximated by B3LYP and ROMP2 calculations reasonably well and showed ±13 and 16 kJ mol^{-1} root-mean-square deviations (rmsd), respectively (Table 4). Since the deviations for B3LYP and ROMP2 energies were of similar magnitude but showed opposite signs, an

Table 4. Dissociation and Adiabatic Ionization Energies of Nitrobenzene and Nitrosobenzene

	reaction enthalpy[a−c]							
method	**1**	**2**	**3**	**4**	**5**	**6**	**7**	rmsd
B3LYP/6-31+G(d,p)	286	223	182	244	63	939	785	10
B3LYP/6-311+G(2df,p)	281	215	182	247	65	942	780	11
PMP2/6-311+G(2df,p)	329	253	145	221	76	965	808	26
ROMP2/6-311+G(2df,p)	310	235	151	227	76	959	813	19
PMP2/6-311+G(3df,2p)	331	255	146	222	76	*d*	810	29
ROMP2/6-311+G(3df,2p)	312	236	152	229	76	959	815	19
QCISD(T)/6-311+G(2df,p)								
UMP2	320	239	152	233	81			18
PMP2	327	245	153	234	82			21
ROMP2	319	237	152	234	82			17
QCISD(T)/6-311+G(3df,2p)								
UMP2	323	241	153	235	82			19
PMP2	329	247	154	236	82			22
ROMP2	323	238	154	236	82			18
B3-PMP2/6-311+G(2df,p)	305	234	163	234	71	953	794	10
B3-ROMP2/6-311+G(2df,p)	296	225	166	237	71	950	797	9
exp.	295	228	171	246	76	954	781	
		±10	±10				±4	

[a] Including B3LYP/6-31+G(d,p) zero-point corrections and 298 K enthalpy corrections. [b] In kJ mol^{-1}. [c] Reaction 1: $C_6H_5NO_2 \rightarrow C_6H_5^{\bullet} + NO_2^{\bullet}$. Reaction 2: $C_6H_5NO \rightarrow C_6H_5^{\bullet} + NO^{\bullet}$. Reaction 3: $C_6H_6 + NO_2^{\bullet} \rightarrow C_6H_5NO_2 + H^{\bullet}$. Reaction 4: $C_6H_6 + NO^{\bullet} \rightarrow C_6H_5NO + H^{\bullet}$. Reaction 5: $C_6H_5NO_2 + NO \rightarrow C_6H_5NO + NO_2$. Reaction 6: $C_6H_5NO_2 \rightarrow C_6H_5NO_2^{+\bullet}$. Reaction 7: $C_6H_5NO \rightarrow C_6H_5NO^{+\bullet}$. [d] The UHF calculations did not converge.

improved agreement due to error cancellation was achieved for B3-PMP2 and B3-ROMP2 energies which agreed with experimental data within ±10 and ±9 kJ mol^{-1} rmsd, respectively. Interestingly, the performance of B3-ROMP2 with the present test set was substantially better than that of the "best" composite QCISD(T)/6-311+G(3df,2p) procedure that showed rmsd of (18 kJ mol^{-1} (Table 4). The B3-ROMP2 data were therefore used to evaluate the energetics of radicals **1**−**5**. The agreement for

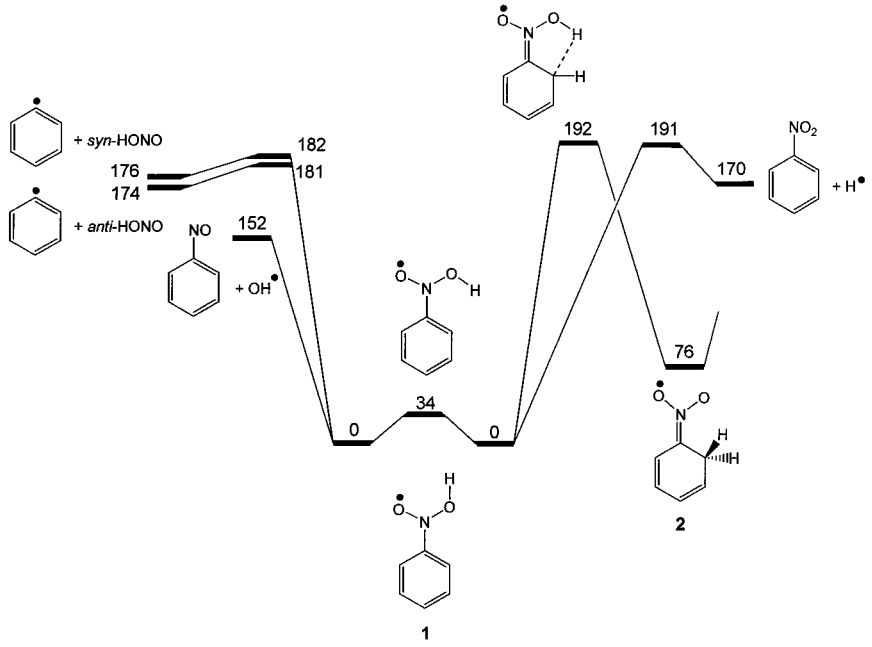

Figure 4. B3-ROMP2 potential energy diagram for **1**. 0 K energies in kJ mol^{-1}.

Table 5. Ionization and Recombination Energies of Nitrobenzene Radicals

	ionization and recombination energies[a,b]			
method	**1**	**2**	**3**	**5**
B3LYP/6-31+G(d,p)	7.30	7.72	7.42	7.65
B3LYP/6-311+G(2df,p)	7.28 (7.07)[c]	7.71	7.43	7.65
PMP2/6-311+G(2df,p)	6.95 (6.74)[c]	7.53	7.44	7.67
ROMP2/6-311+G(2df,p)	7.05 (6.82)[c]	7.57	7.39	7.65
PMP2/6-311+G(3df,2p)	6.97	7.55	7.46	7.69
ROMP2/6-311+G(3df,2p)	7.07	7.59	7.40	7.67
B3-PMP2/6-311+G(2df,p)	7.12 (6.90)[c]	7.62	7.43	7.66
B3-ROMP2/6-311+G(2df,p)	7.17 (6.95)[c]	7.64	7.41	7.65

[a] The adiabatic ionization energies include B3LYP/6-31+G(d,p) zero-point corrections. [b] In units of electronvolts. [c] Vertical recombination energies in parentheses.

the ion energetics was reasonably good for both B3-PMP2 and B3-ROMP2 where the rmsd were (19 and (21 kJ mol^{-1}, respectively. The major sources of error were from the reaction enthalpies involving the nitrosobenzene cation-radical that differed from the experiment-derived values by 20−40 kJ mol^{-1} (Table 1) We note that the experimental adiabatic ionization energy of nitrosobenzene which is included in the enthalpy of formation of $C_6H_5NO^{+\bullet}$ was extrapolated from a poorly resolved band in the photoelectron spectrum[60] and may be underestimated. A comparable fit for the ion energies was obtained from the B3LYP data alone which showed rmsd of 16−22 kJ mol^{-1} (Table 1).

The ion and radical energetics are connected through adiabatic ionization energies (IE_a) and vertical recombination energies (RE_v). The differences between the IE_a and RE_v values provide estimates of vibrational excitation in radicals formed by vertical electron transfer. The calculated IE_a and RE_v are summarized in Table 5 for selected species. The data showed that **1** had a lower ionization energy than the nitrocyclohexadienyl radicals **2**, **3**, and **5**. This was mostly due to the substantial stabilization of ion $\mathbf{1}^+$ relative to the ring protonated nitrobenzene ions $\mathbf{2}^+$−$\mathbf{5}^+$ (cf. Table 1). The Franck−Condon effects in vertical neutralization of $\mathbf{1}^+$ were small and resulted in excitations of <20 kJ mol^{-1}, as documented by the calculated $IE_a - RE_v$ values (Table 5).

Transition states were sought for several dissociations and isomerizations of **1**, as summarized in a potential-energy diagram (Figure 4). The lowest-energy dissociation of **1** was cleavage of the N−OH bond that required 145−152 kJ mol^{-1} at the B3-PMP2 and B3-ROMP2 thresholds, respectively (Table 6). The B3-PMP2 potential energy profile along the N−OH coordinate was studied by stepwise calculations and showed a continuously endothermic dissociation with no barrier for the reverse addition of OH$^\bullet$ to nitrosobenzene. Dissociation of the C-1−NO_2H bond in **1** showed two isomeric transition states leading to the formation of the *syn* and *anti* rotamers of HONO. Since **1** exists as a *syn* isomer only, branching into the isomeric transition states occurred along the dissociation coordinate at a C-1−NO_2H bond length of about 1.6 Å, beyond which distance the intermediate *syn* and *anti* structures each showed positive force constants for OH rotation that indicated separate dissociation paths. The activation energies for the addition of phenyl radical to *syn*- and *anti*-HONO were small, 6 and 7 kJ mol^{-1}, respectively, by B3-ROMP2 calculations. For energies obtained at the other levels of theory see Table 6.

Dissociation of the O−H bond in **1** required 165 and 170 kJ mol^{-1} at the B3-PMP2 and B3-ROMP2 thresholds, respectively (Table 6). The dissociation path was studied in detail and is used here as a difficult case in point to illustrate the approach we also adopted for C−H bond cleavages in **2**−**5** that showed better behavior. Full optimizations with B3LYP/6-31+G(d,p) provided a continuous potential energy profile with a first-order saddle point at d(O−H) = 1.84 Å (Figure 5). Single-point energy calculations along the reaction path showed maxima at d(O−H) = 1.80, 1.6, and 1.5 Å, for B3LYP, PMP2, and ROMP2, respectively, which were displaced toward shorter O−H distances compared with the fully optimized saddle point geometry. The averaged B3-PMP2 and B3-ROMP2 energies peaked out at 1.7 Å, and following ZPVE corrections were used to estimate transition state energies. The potential energy profile from the B3-PMP2 and B3-ROMP2 calculations showed a rather sharp curvature around the saddle point region (Figure 5), which

(60) (a) Rabalais, J. W.; Colton, R. J. *J. Electron Spectrosc. Relat. Phenom.* **1973**, *1*, 83. (b) Egdell, R.; Green, J. C.; Rao, C. N. R.; Gowenlock, B. G.; Pfab, J. *J. Chem. Soc., Faraday Trans. 2* **1975**, 988.

Table 6. Dissociation and Activation Energies of **1**

	reaction and activation enthalpy[a–c]							
method	**1**	**2**	**3**	**4**	**5**	**6**	**7**	**8**
B3LYP/6-31+G(d,p)	168	173	167	173	199	205	141	20
B3LYP/6-311+G(2df,p)	166	172	164	171	193	200	145	14
PMP2/6-311+G(2df,p)	189	194	187	194	137	209	146	−5
ROMP2/6-311+G(2df,p)	186	198	185	191	146	181	159	−2
PMP2/6-311+G(3df,2p)	189		188		141	221	147	−2
ROMP2/6-311+G(3df,2p)	186	188	185		151	174	161	1
QCISD(T)/6-311+G(2df,p)								
UMP2	159	167	157		153	190	118	4
PMP2	164	169	161		149	170	113	−1
ROMP2	165	176	162		159	198	124	10
QCISD(T)/6-311+G(3df,2p)								
UMP2	159	167	157		157	186	119	6
PMP2	164	168	161		154	181	114	2
ROMP2	165	168	162		164	191	125	13
B3-PMP2/6-311+G(2df,p)	178	183	176	183	165	205	145	4
B3-ROMP2/6-311+G(2df,p)	176	182	174	181	170	191	152	6
	178[d]		176[d]		173[d]		156[d]	6.5[d]

[a] Including B3LYP/6-31+G(d,p) zero-point corrections. [b] In units of kJ mol^{-1} at 0 K. [c] Reaction 1: $C_6H_5NO_2H^\bullet \rightarrow C_6H_5^\bullet$ + *syn*-HONO. Reaction 2: $C_6H_5NO_2H^\bullet \rightarrow$ **TS**($C_6H_5^\bullet$...*syn*-HONO). Reaction 3: $C_6H_5NO_2H^\bullet \rightarrow C_6H_5^\bullet$ + *anti*-HONO. Reaction 4: $C_6H_5NO_2H^\bullet \rightarrow$ **TS**($C_6H_5^\bullet$...*anti*-HONO). Reaction 5: $C_6H_5NO_2H^\bullet \rightarrow C_6H_5NO_2 + H^\bullet$. Reaction 6: $C_6H_5NO_2H^\bullet \rightarrow$ **TS**($C_6H_5NO_2$...$H^\bullet$). Reaction 7: $C_6H_5NO_2H^\bullet \rightarrow C_6H_5NO + OH^\bullet$. Reaction 8: $C_6H_5NO_2H^\bullet \rightarrow C_6H_6 + NO_2^\bullet$. [d] 298 K energies.

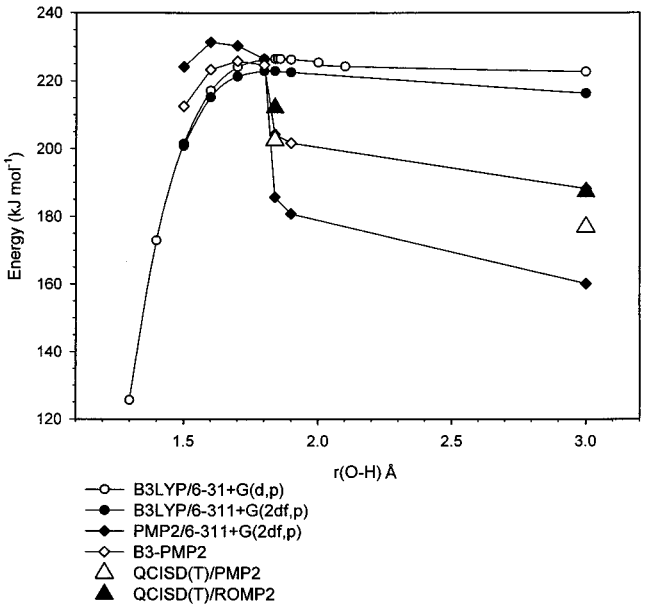

Figure 5. Potential energy profiles along the O−H coordinate in **1**.

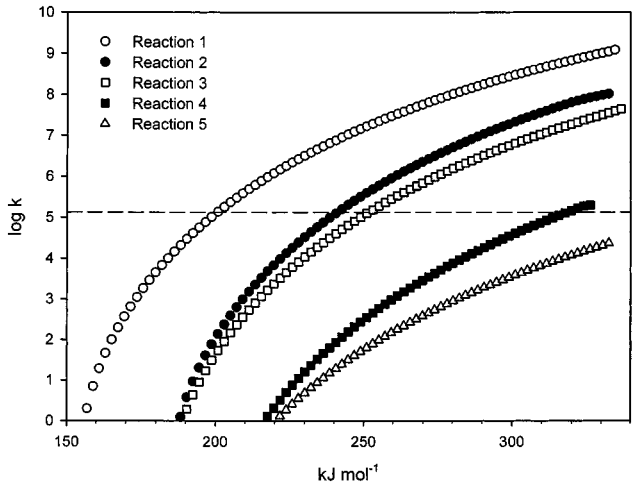

Figure 6. RRKM rate constants (log k versus internal energy) for dissociations of **1**. Reaction 1: **1** → $C_6H_5NO + OH^\bullet$. Reaction 2: **1** → $C_6H_5^\bullet$ + *syn*-HONO. Reaction 3: **1** → $C_6H_5^\bullet$ + *anti*-HONO. Reaction 4: **1** → $C_6H_5NO_2 + H^\bullet$. Reaction 5: **1** → **2**. The dashed line at log $k = 5.12$ corresponds to rate constants for 50% dissociation on the experimental time scale.

was caused by the large energy differences between the transition state and products calculated by PMP2 and ROMP2. Single point energies were also calculated with the effective QCISD(T)/6-311+G(3df,2p) at the saddle point geometry, but the considerable time and memory requirements of these calculations made reaction path mapping impractical. The transition state energy from the effective QCISD(T) single-point calculations (cf. eq 1) were slightly lower than that from B3-MP2 calculations (Table 6).

The unimolecular isomerization of **1** to **2** was also accompanied by a sizable energy barrier. The B3-PMP2 and B3-ROMP2 barriers for the **1** → **2** isomerization (190 and 192 kJ mol^{-1}, respectively) agreed well with those from effective QCISD(T)/6-311+G(3df,2p) (194 and 187 kJ mol^{-1}, respectively, **TS12**, Table 7). According to the calculated dissociation and isomerization energetics, the formation of $C_6H_5NO + OH^\bullet$ should be the preferred unimolecular reaction of **1** at all levels of theory.

The calculated transition state energies were used to calculate unimolecular rate constants (k_{uni}) for the above-discussed reactions using the RRKM theory. The k_{uni} values that were based on the B3-ROMP2 transition state energies are shown in Figure 6. The k_{uni} that were based on B3-PMP2 energies showed very similar trends and will not be discussed separately. The calculated k_{uni} strongly indicated that *loss of OH should be the dominant dissociation* of **1** from the dissociation threshold up to the highest internal energy studied (330 kJ mol^{-1}). Losses of *syn*- and *anti*-HONO became competitive with the loss of OH only at the highest internal energies and could account for up to 10% of the total dissociation of **1** having >300 kJ mol^{-1} internal energies. Interestingly, dissociation through the *syn*-transition state that had a slightly higher energy in the transition state was calculated to be faster than that for the *anti*-isomer. In contrast, loss of the hydrogen atom from the NO_2H group and isomerization to **2** were calculated to be 3−5 orders of magnitude slower than loss of OH and therefore should not be competitive in dissociations of **1** in its ground electronic state. The unimolecular dissociations of **1** showed substantial kinetic shifts caused by the finite time scale of the experimental

Table 7. Dissociation and Activation Energies of Wheland Intermediates

	reaction and activation enthalpies[a−c]											
method	**1**	**2**	**3**	**4**	**5**	**6**	**7**	**8**	**9**	**10**	**11**	**12**
B3LYP/6-31+G(d,p)	123	134	100	115	120	133	95	122	−84	−0.2	179	154
B3LYP/6-311+G(2df,p)	115	130	93	112	113	128	89	119	−91	−0.8	180	152
PMP2/6-311+G(2df,p)	69	110	54	99	64	107	50	103	−93	8	199	162
ROMP2/6-311+G(2df,p)	72	112	48	94	59	111	48	102	−101	7.5	203	156
PMP2/6-311+G(3df,2p)	73	113	58	101	69	115	55	106	−89		227	162
ROMP2/6-311+G(3df,2p)	77	105	52	87	64	106	53	97	−97	8	205	157
QCISD(T)/6-311+G(3df,2p)												
UMP2	89	126	75	119	88	128	76	127	−74		193	
PMP2	88	128	73	120	86	128	73	128	−78		194	
ROMP2	100	131	82	121	94	129	82	128	−69		187	
B3-PMP2/6-311+G(2df,p)	92	120	73	105	89	118	69	111	−92	3.6	190	157
B3-ROMP2/6-311+G(2df,p)	93	120	70	104	86	117	68	107	−95	3.4	192	155
	98[d]		75[d]		91[d]		72[d]		−94[d]			

[a] Including B3LYP/6-31+G(d,p) zero-point corrections. [b] In units of kJ mol^{-1} at 0 K. [c] Reaction 1: **2** → $C_6H_5NO_2$ + H$^\bullet$. Reaction 2: **2** → **TS**(*ortho*-H···$C_6H_5NO_2$). Reaction 3: **3** → $C_6H_5NO_2$ + H$^\bullet$. Reaction 4: **3** → **TS**(*meta*-H···$C_6H_5NO_2$). Reaction 5: **4** → $C_6H_5NO_2$ + H$^\bullet$. Reaction 6: **4** → **TS**(*para*-H···$C_6H_5NO_2$ + H$^\bullet$). Reaction 7: **5** → $C_6H_5NO_2$ + H$^\bullet$. Reaction 8: **5** → **TS**(*ipso*-H···$C_6H_5NO_2$). Reaction 8: **5** → C_6H_6 + NO_2. Reaction 10: **5** → **TS**(*ipso*-C_6H_6...NO_2). Reaction 11: **TS**(**12**). Reaction 12: **TS**(**23**). [d] 298 K enthalpies.

measurements. These are shown in Figure 6 at log k_{uni} = 5.12 corresponding to 50% dissociation during the 5.3 μs flight time of **1**. The lowest-energy dissociation of **1** was estimated to have a 48 kJ mol^{-1} kinetic shift, which should enhance the kinetic stability of **1**.

Are the RRKM rate constants compatible with the experimental rate parameters? The variable-time measurements pointed to neutral dissociations of **1** forming both C_6H_5NO and $C_6H_5^\bullet$. In contrast, the calculated threshold energies suggested that $C_6H_5^\bullet$ could be formed competitively with C_6H_5NO only from highly excited **1**. However, C_6H_5NO formed by loss of OH was found to dissociate rapidly following reionization to produce $C_6H_5^+$, as evidenced by a large rate parameter for the ion dissociation. Hence, the apparent rate parameter for **1** → $C_6H_5^\bullet$ → $C_6H_5^+$ could in part be due to a rate-determining neutral dissociation **1** → C_6H_5NO followed by fast dissociation of reionized $C_6H_5NO^+$. In this way the temporal profile for the formation of $C_6H_5^+$ can show dependence on the time scale for the slower neutral dissociation.

What drives the unimolecular dissociations of **1**? Figure 6 shows that radicals **1** dissociating on the 5.3 ms time scale of the experiment must have substantial internal energies, estimated at 180−200 kJ mol^{-1} depending on the level of theory used, to access the lowest energy channel. On average, the internal energy of **1** is composed of the neutral precursor thermal energy (46 kJ mol^{-1} for vibrational and rotational enthalpy of nitrobenzene at 523 K), a 80% fraction of the protonation exothermicity[35b,61] (17 kJ mol^{-1}) and the Franck−Condon energy (E_{FC}) resulting from vertical electron transfer. Note, however, that excitation through Franck−Condon effects was remarkably small in vertically formed **1**, for example 14 kJ mol^{-1} by B3-ROMP2 (Table 5). Clearly, the sum of the foregoing energy terms, that is 46 + 17 + 14 = 77 kJ mol^{-1}, falls short to provide the vibrational excitation needed for the lowest-energy dissociation of **1**. This leads to the logical conclusion that **1** formed in the ground electronic state could not dissociate. Hence, the neutral dissociations must have been driven by formation upon collisional electron transfer of excited electronic states that decayed non-radiatively to a vibrationally excited ground state, or underwent state-specific dissociations to yield the observed products.

Excited States of 1. Excited states in **1** were addressed by complete active space (CASSCF(5,5)/6-31G(d,p)) and configuration-interaction singles (CIS/6-311+G(2df,p)) calculations to provide a rough estimate of excitation energies and radiative lifetimes. The active space for the CASSCF calculations included the top three occupied π-molecular orbitals and two unoccupied π-orbitals from the virtual orbital space. Energies were calculated for **1** produced by vertical electron capture in $\mathbf{1}^+$ and for the relaxed structure of the ground-state radical. The energies for the relaxed and vertically formed **1** were very similar and need not be discussed separately. The CASSCF excitation energy for the $X \rightarrow A$ transition (3.42 eV) was compatible with a band in the UV absorption spectrum of the putative [nitrobenzene + H] adduct (3 eV).[16−18] The *A*, *B*, and *C* excited states were due to excitation of a valence electron to the virtual orbital space. These outer excited states from the CIS calculations were relevant to the formation of **1** by femtosecond electron transfer. The *A*, and *C* states had nanosecond lifetimes for radiative transitions to the *X* state. Hence, these states were too short-lived to undergo dissociations on the microsecond time scale. In contrast, the $B \rightarrow X$ transition was dipole forbidden ($|R_{mn}| = 4 \times 10^{-4}$ au^2) and the ensuing >10 μs radiative lifetime should allow it to participate in unimolecular dissociations. The *B* state had a sufficient energy (calculated as ∼520 kJ mol^{-1} above the *X* state) to drive competitive dissociations by N−O, C−N, and O−H bond cleavages following internal conversion to a vibrationally excited *X* state. Furthermore, direct dissociation from the *B* state to excited electronic states of the dissociation products appears to be energetically possible for the formation of $(C_6H_5^\bullet)^*$ + HONO. The excited states of $C_6H_5^\bullet$ are known to be 2.47, 4.51, and 5.00 eV above the ground state,[62−64] so that formation from **1** of $(C_6H_5^\bullet)^*$ + HONO required ∼413 kJ mol^{-1} and was accessible from the *B* state of **1**. In contrast, the formation of $(C_6H_5NO)^*$ + OH$^\bullet$ is estimated to require 590 kJ mol^{-1} (ref 62) which could not be supplied by the excitation energy of the *B* state alone. Loss of H$^\bullet$ to form an excited state of $(C_6H_5NO_2)^*$ was estimated[62] to require ∼600 kJ mol^{-1} which was also above the *B* state energy.

(61) Uggerud, E. *Adv. Mass Spectrom.* **1995**, *13*, 53.

(62) Calculated on the basis of excitation energies from the corresponding UV absorption maxima. The λ_{max} values used were: nitrobenzene (240 and 280 nm),[62] nitrosobenzene (270 and 290 nm),[63a] and phenyl radical (248, 275, and 502 nm).[63a,b]

(63) (a) Nagakura, S.; Kojima, M.; Maruyama, Y. *J. Mol. Spectrosc.* **1964**, *13*, 174. (b) Glenewinkel-Meyer, T.; Crim, F. F. *J. Mol. Struct. (THEOCHEM)* **1995**, *337*, 209.

(64) (a) Ikeda, N.; Nakashima, N.; Yoshihara, K. *J. Am. Chem. Soc.* **1985**, *107*, 3381. (b) Porter, G.; Ward, B. *Proc. R. Soc. Ser. A, Math. Phys. Sci.* **1965**, *287*, 457.

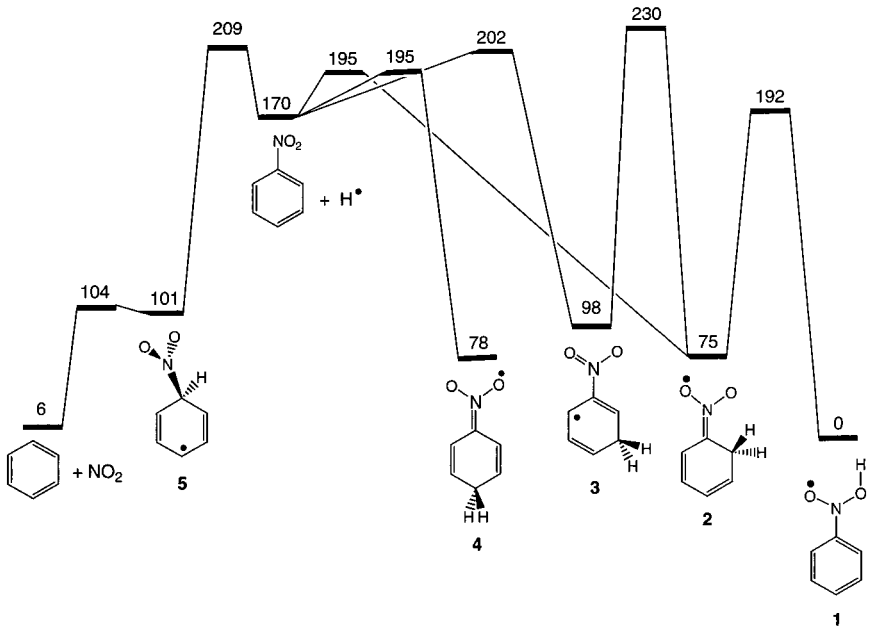

Figure 7. B3-ROMP2 potential energy diagram for Wheland intermediates **2**−**5**. 0 K energies in kJ mol^{-1}.

Summarizing the discussion of excited states, the experimentally observed loss of OH from **1** can be driven by the formation of a metastable *B* state that undergoes internal conversion to a vibrationally excited, dissociative *X* state. Since the loss of OH is predicted by RRKM calculations to be very fast at excitation energies >250 kJ mol^{-1} (Figure 6), the measured μs rate parameter must correspond to $B \rightarrow X$ internal conversion as the rate-determining step. The loss of *syn*- or *anti*-HONO from **1**, which could not be distinguished experimentally from a stepwise dissociation, $\mathbf{1} \rightarrow C_6H_5NO \rightarrow C_6H_5NO^{+\bullet} \rightarrow C_6H_5^+ +$ NO (vide supra), can occur from high vibrational states of the *X* state of **1**, where the C−N bond cleavages become competitive with the N−O bond cleavage (Figure 6). In addition, direct dissociation from the *B* state of **1** to form an excited state of $C_6H_5^\bullet$ appears to be energetically possible and can contribute to the observed μs kinetics.

Wheland Intermediates 2−5. The energetics of radicals **2**−**5** were addressed by B3-PMP2 and B3-ROMP2 calculations (Table 3). The calculated order of stabilities, *ortho* > *para* > *meta* > *ipso* was in qualitative accord with Wheland's predictions for nitrobenzene reactivity in radical addition.[8] The *ortho*, *meta*, and *para* isomers **2**−**4** were substantially stable with respect to isomerizations and dissociations (Table 7). For example, the isomerizations $\mathbf{2} \rightarrow \mathbf{1}$, $\mathbf{2} \rightarrow \mathbf{3}$, and loss of an *ortho*-hydrogen atom required activation energies of 117, 155, and 120 kJ mol^{-1}, respectively (Figure 7). In contrast, the *ipso* isomer **5** was only marginally bound with respect to loss of NO_2 which was exothermic by 95 kJ mol^{-1} at 298 K (Table 7). The energy barrier from **5** to the transition state for loss of NO_2 was only 3 kJ mol^{-1} suggesting very facile dissociation. The marginal stability of **5** was indicated by the optimized structure which showed a long C-1−N bond (1.610 Å, Figure 3). In summary, the *ortho*, *meta*, and *para* Wheland intermediates **2**−**4** were predicted to be sufficiently stable to be prepared as separate structures in the gas phase. In contrast, the *ipso* isomer **5** existed in a very shallow potential energy minimum and was predicted to dissociate rapidly to benzene and nitrogen dioxide.

Hydrogen Atom Addition to Nitrobenzene. Of particular interest with respect to radical additions to nitrobenzene were the activation energies for loss of hydrogen atom from **1** and **2**−**5** and, by microscopic reversibility, the barriers for hydrogen atom additions to the nitro group and the ring positions. The B3-PMP2 and B3-ROMP2 calculations preferred addition to the *ortho* position that had the smallest activation energy $E_a =$ 25−28 kJ mol^{-1} (Table 8). In contrast, effective QCISD(T)/6-311+G(3df,2p) predicted addition to the nitro group to be the lowest activation energy reaction of $E_a =$ 27−28 kJ mol^{-1} (Table 8). This discrepancy was caused by the poor performance of MP2 calculations in treating the transition state energy for the H atom addition to the nitro group. The deficiencies in the MP2 energies largely canceled out in the basis set expansion included in the effective QCISD(T)/6-311+G(3df,2p) energies which were within 5 kJ mol^{-1} of the QCISD(T)/6-31G(d,p) values. Error cancellation was less efficient in the B3-PMP2 and B3-ROMP2 energies where the high activation barriers from the MP2 calculations were not compensated by the underestimated values from the B3LYP calculations. In contrast, the activation energies for additions to the ring positions by QCISD(T)/6-311+G(3df,2p) were consistently 12−15 kJ mol^{-1} and 7.7−8.8 kJ mol^{-1} *greater* than those from B3-PMP2 or B3-ROMP2, respectively. (Table 8). However, relative to each other, the activation energies and rate constants showed very similar trends for the four series of calculations. For example, the branching ratios for additions to the *ortho*, *meta*, *para*, and *ipso* positions were 76, 7, 17, and 0.1% from QCISD(T)-ROMP2 calculations in essential agreement with the B3-ROMP2 data (72, 11, 18, and 0.1%, respectively, Table 8).

The calculated absolute rate constants for H atom addition to the nitro group at 273 K ranged from 2.5×10^7 to 7.4×10^7 s^{-1} mol^{-1} cm^3, not including the statistical factor due to the presence of two equivalent oxygen atoms in nitrobenzene. These values were in reasonable agreement with the single experimental rate constant that was reported as $k = 1.53 \times 10^7$ s^{-1} mol^{-1} cm^3 at an unspecified temperature.[18] The addition was postulated to produce a nitrocyclohexadienyl radical adduct of an unspecified structure.[18] In contrast, the present calculations suggest that *formation of the phenylnitronic radical should be preferred*.

The calculated relative branching ratios for H atom addition to the *ortho*, *meta*, and *para* positions in nitrobenzene correlated with the product yields in other radical additions, for example those of methyl and phenyl radicals.[4,10−12] It should be noted

Table 8. Activation Energies and Rate Constants for Hydrogen Atom Addition to Nitrobenzene

position	method	E_{TS}[a]	E_{Arrh}[a,b]	log A[b]	log k_{250}[c]	log k_{298}	log k_{350}	k_{rel}[d]
ortho	B3PMP2	27.9	28.5	12.90	6.95	7.91	8.67	0.64
	B3ROMP2	25.3	25.8		7.50	8.37	9.06	0.72
	QCISD(T)							
	UMP2	36.7	37.3		5.11	6.37	7.35	0.80
	PMP2	40.0	40.6		4.41	5.78	6.85	0.77
	ROMP2	33.2	33.7		5.85	6.99	7.88	0.76
meta	B3PMP2	31.8	32.3	12.91	6.16	7.25	8.11	0.14
	B3ROMP2	30.2	30.7		6.50	7.54	8.35	0.11
	QCISD(T)							
	UMP2	43.9	44.4		3.63	5.13	6.30	0.05
	PMP2	46.8	47.3		3.02	4.62	5.86	0.05
	ROMP2	39.0	39.5		4.65	5.98	7.03	0.07
para	B3PMP2	29.1	29.7	12.95	6.75	7.75	8.53	0.22
	B3ROMP2	27.2	27.8		7.13	8.07	8.81	0.18
	QCISD(T)							
	UMP2	39.3	39.8		4.62	5.96	7.01	0.16
	PMP2	42.3	42.9		3.99	5.43	6.56	0.17
	ROMP2	35.4	36.0		5.42	6.63	7.59	0.17
ipso	B3PMP2	41.5	41.4	12.68	4.02	5.41	6.50	0.002
	B3ROMP2	38.9	38.9		4.55	5.86	6.88	0.001
	QCISD(T)							
	UMP2	51.5	51.5		1.92	3.65	5.00	0.0008
	PMP2	55.1	55.0		1.17	3.03	4.47	0.0007
	ROMP2	46.6	46.6		2.94	4.51	5.73	0.001
NO_2	B3PMP2	37.4	38.9	13.28	5.14	6.45	7.49	
	B3ROMP2	32.4	33.7		6.24	7.38	8.27	
	QCISD(T)							
	UMP2	29.4	30.7		6.86	7.90	8.72	
	PMP2	27.6	28.9		7.24	8.21	8.98	
	ROMP2	27.0	28.3		7.37	.33	9.08	

[a] Activation energies in kJ mol^{-1}. [b] From Arrhenius plots of log k versus $1/T$. Rate constants in mol^{-1} cm^3 s^{-1} at indicated absolute temperatures. [d] Fractions for H atom additions to the *ortho*, *meta*, *para*, and *ipso* positions in nitrobenzene.

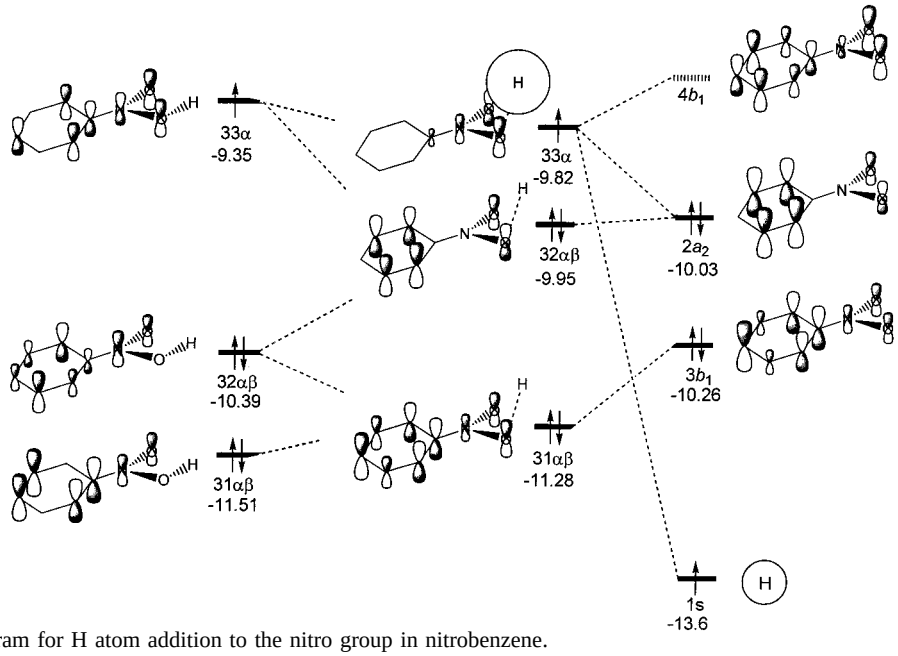

Figure 8. Orbital diagram for H atom addition to the nitro group in nitrobenzene.

that a methyl radical addition to the nitro group in nitrobenzene would not yield a stable adduct but would likely produce nitrosobenzene by a mildly endothermic elimination of a methoxyl radical (eq 5).

$$C_6H_5NO_2 + CH_3^{\bullet} \rightarrow C_6H_5NO + OCH_3^{\bullet}$$
$$\Delta H_{rxn,298} = 11 \text{ kJ mol}^{-1} \quad (5)$$

Likewise, alkyl or phenyl radical addition to the *ipso* position in nitrobenzene is predicted by the present calculations to result in expulsion of NO_2 to yield an alkyl benzene or diphenyl.

Why are there activation barriers to hydrogen atom additions to nitrobenzene? The answer to this question was sought by examining the interactions between the unpaired electron in the 1s orbital of the reacting hydrogen atom and the orbital system of nitrobenzene, as shown for the addition to the nitro group (Figure 8) and *ipso* position (Figure 9). The 1s electron of the hydrogen atom can interact with the unoccupied $4b_1$ orbital in nitrobenzene, which has substantial expansion coefficients at the oxygen atoms, so that the unpaired electron enters the developing singly occupied orbital (SOMO, 33a) in the transition state of the addition. However, the nodal properties within the

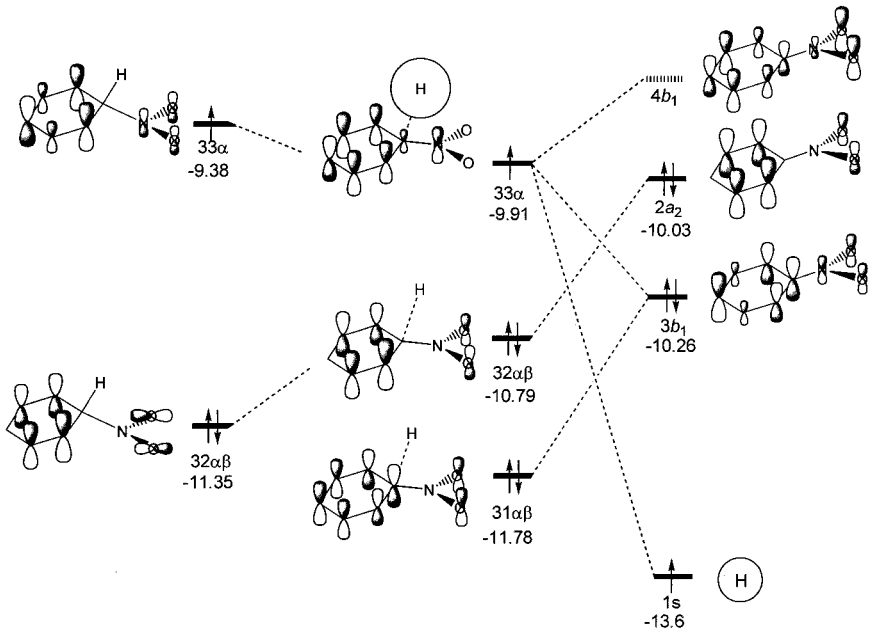

Figure 9. Orbital diagram for H atom addition to the *ipso* position in nitrobenzene.

nitro group of the SOMO in the transition state differ from those in the nitrobenzene $4b_1$ orbital (Figure 8). The SOMO develops by mixing the unoccupied $4b_1$ orbital with the $2a_2$ orbital (HOMO) of appropriate nodal properties. However, the HOMO is doubly occupied and mixing it with the $4b_1$ orbital increases electron energy, which results in an activation barrier.

Addition to the *ipso* position shows a different correlation (Figure 9). Interaction of the hydrogen atom 1s electron with the $4b_1$ orbital in nitrobenzene preserves the orbital symmetry, for example $B_1 \rightarrow A'$, in the transition state, and does not involve the HOMO ($2a_2$) which has an A_2 symmetry. However, the nodal properties of the SOMO in the transition state require mixing of the $4b_1$ and $3b_1$ orbitals, indicating valence electron excitation (Figure 9). Hydrogen atom addition to the *para* position in nitrobenzene showed orbital correlations that were analogous by symmetry to those for the *ipso* addition. The reasons for activation barriers in additions to the *ortho* and *meta* positions in nitrobenzene are somewhat subtler. In both the *ortho* and *meta* additions, the $3b_1$ and $2a_2$ doubly occupied nitrobenzene orbitals must mix to provide the $31\alpha\beta$ and $32\alpha\beta$ occupied orbitals in the transition states that further correlate with occupied orbitals in the adducts **2** and **3**, respectively. In addition, mixing of the occupied $2a_2$ orbital with the unoccupied $4b_1$ and/or $5b_1$ orbitals is also necessary to achieve appropriate nodalities of the SOMO's in the transition states for the *ortho* and *meta* addition. The ensuing electronic excitation contributes to the activation energy but it can be moderated by the decrease or increase of electronic energy due to mixing of the $3b_1$ and $2a_2$ orbitals.

Conclusions

Phenylnitronic radical **1** was generated in the gas phase and shown to be kinetically and thermodynamically stable. The lowest-energy dissociation of **1** was loss of OH to form nitrosobenzene which occurred at the reaction thermochemical threshold without a reverse barrier. However, **1** prepared by collisional electron transfer did not have sufficient internal energy to dissociate. The observed dissociations were driven by the formation of excited electronic states. A metastable *B* state was identified by calculations that had both a long radiative lifetime and sufficient energy to participate in unimolecular dissociations. The calculated branching ratios for hydrogen atom additions to the *ortho*, *meta*, and *para* positions in nitrobenzene correlated well with the experimental branching ratios for additions of small radicals. Radicals derived from nitrobenzene represent computationally difficult systems.

Despite the high-level of theory employed in this work, uncertainties remain as to the relative rates of hydrogen atom additions to the nitro group and the ring positions.

Acknowledgment. Support of this work by the National Science Foundation (Grant CHE-9712570) is gratefully acknowledged. The computations were performed at the Department of Chemistry Computer Facility that received generous funding from NSF (Grant CHE-9808182). We thank Dr. Martin Sadílek for technical assistance with CAD spectra measurements and a reviewer for suggesting experiments with ion−molecule reactions.

Supporting Information Available: Tables of total energies, optimized geometries, and harmonic frequencies (PDF). This material is available free of charge via the Internet at http://pubs.acs.org.

JA001229H